A new dinosaur with theropod affinities from the Late Triassic Santa Maria Formation, South Brazil

Marsola, Julio; Bittencourt, Jonathas; Butler, Richard; Da Rosa, Atila; Sayao, Juliana; Langer, Max

DOI:
10.1080/02724634.2018.1531878

A new dinosaur with theropod affinities from the Late Triassic Santa Maria Formation, South Brazil

JÚLIO C. A. MARSOLA,[*,1, 2], JONATHAS SOUZA BITTENCOURT,[3] RICHARD J. BUTLER,[2] ÁTILA A. S. DA ROSA,[4] JULIANA M. SAYÃO,[5] and MAX C. LANGER[1]

[1]Laboratório de Paleontologia, FFCLRP, Universidade de São Paulo, Ribeirão Preto-SP, 14040-901, Brazil, juliomarsola@gmail.com, mclanger@ffclrp.usp.br

[2]School of Geography, Earth and Environmental Sciences, University of Birmingham, Birmingham, B15 2TT, U.K., r.butler.1@bham.ac.uk

[3]Departamento de Geologia, Universidade Federal de Minas Gerais, Belo Horizonte-MG, 31270-901, Brazil, sigmaorionis@yahoo.com.br

[4] Laboratório de Estratigrafia e Paleobiologia, Departamento de Geociências, Universidade Federal de Santa Maria, Santa Maria-RS, 97.105-900, Brazil, atila@smail.ufsm.br

[5]Laboratório de Paleobiologia e Microestruturas, Núcleo de Biologia, Centro Acadêmico de Vitória, Universidade Federal de Pernambuco, Vitória de Santo Antão-PE, 52050-480, Brazil, jmsayao@gmail.com

[*]Corresponding author

ABSTRACT—The Late Triassic (Carnian) upper Santa Maria Formation of south Brazil has yielded some of the oldest unequivocal records of dinosaurs. Here, we describe a new saurischian dinosaur from this formation, *Nhandumirim waldsangae* gen. et sp. nov., based on a semi-articulated skeleton, including trunk, sacral, and caudal vertebrae, one chevron, right ilium, femur, partial tibia, fibula, and metatarsals II and IV, as well as ungual and non-ungual phalanges. The new taxon differs from all other Carnian dinosauromorphs through a unique combination of characters, some of which are autapomorphic: caudal centra with sharp longitudinal ventral keels; brevis fossa extending for less than three-quarters of the ventral surface of the postacetabular ala of the ilium; dorsolateral trochanter ending well distal to the level of the femoral head; distal part of the tibia with a mediolaterally extending tuberosity on its cranial surface and a tabular caudolateral flange; conspicuous craniomedially oriented semi-circular articular facet on the distal fibula; and a straight metatarsal IV. This clearly distinguishes *Nhandumirim waldsangae* from both *Saturnalia tupiniquim* and *Staurikosaurus pricei*, which were collected nearby and at a similar stratigraphic level. Despite being not fully-grown, the differences between *Nhandumirim waldsangae* and those saurischians cannot be attributed to ontogeny. The phylogenetic position of *Nhandumirim waldsangae* suggests that it represents one of the earliest members of Theropoda. *Nhandumirim waldsangae* shows that some typical theropod characters were already present early in dinosaur evolution, and possibly represents the oldest record of the group known in Brazil.

INTRODUCTION

Dinosaurs are a highly diverse group of archosaurs that emerged in the Late Triassic and are today represented only by the avian lineage. The oldest unequivocal dinosaur fossils are from Carnian deposits of Argentina and Brazil (southwestern Pangaea), which have yielded a diverse fauna of dinosauromorphs (including dinosaurs), pseudosuchians, rhynchosaurs and therapsids (Langer, 2005b; Brusatte et al., 2008 a,b; 2010; Langer et al., 2010a; Martínez et al., 2012, 2016; Benton et al., 2014; Cabreira et al., 2016). Additional but less complete fossils from India and Zimbabwe suggest a wider palaeobiogeographic distribution for the earliest dinosaurs, with the group also occupying the eastern portion of south Pangea (Ezcurra, 2012).

With the exception of the Argentinean dinosaur *Pisanosaurus mertii*, traditionally interpreted as an ornithischian (Casamiquela, 1967; but see Agnolín and Rozadilla, 2017; Baron, 2017), the record of Carnian dinosaurs is restricted to saurischians (*sensu* Gauthier, 1986), with sauropodomorphs being the most speciose clade. Carnian sauropodomorphs are known from the Ischigualasto Formation of Argentina, including *Eoraptor lunensis* (Sereno et al., 1993), *Panphagia protos* (Martínez and Alcober, 2009) and *Chromogisaurus novasi* (Ezcurra, 2010), and the Santa Maria Formation of Brazil, encompassing *Saturnalia tupiniquim* (Langer et al., 1999), *Pampadromaeus barberenai* (Cabreira et al., 2011) and *Buriolestes schultzi* (Cabreira et al., 2016). These early sauropodomorphs comprise more than 50% of the taxonomic diversity of Carnian dinosaurs. Additional coeval saurischians include the herrrasaurids *Herrerasaurus ischigualastensis* (Reig, 1963), *Staurikosaurus pricei* (Colbert, 1970) and *Sanjuansaurus gordilloi* (Alcober and Martínez, 2010), which have been interpreted in different phylogenetic analyses either as theropods or non-

eusaurischian dinosaurs (e.g. Nesbitt and Ezcurra, 2015; Cabreira et al., 2016). *Eodromaeus murphii* (Martínez et al., 2011) from the Ischigualasto Formation has been interpreted as a theropod by several authors (Martínez et al., 2011; Bittencourt et al., 2014; Nesbitt and Ezcurra, 2015), but was recently recovered as a non-eusaurischian dinosaur (Cabreira et al., 2016). Unambiguous theropods are more common in later Triassic (Norian) deposits, as seen in north Pangea dinosaur faunas, like in the Chinle Formation, that are dominated by coelophysids (e.g. Nesbitt et al., 2009; Ezcurra and Brusatte, 2011; Sues et al., 2011; Nesbitt and Ezcurra, 2015).

Here we describe a partial, semi-articulated skeleton of a somatically immature dinosaur from the historic Waldsanga site (Langer, 2005a) of the Santa Maria Formation, south Brazil. This new specimen represents a new genus and species of saurischian dinosaur, and is tentatively assigned here to Theropoda, representing the oldest potential record of this group in Brazil.

Institutional Abbreviations—**AMNH FARB**, American Museum of Natural History, New York, U.S.A.; **BRSMG**, Bristol Museum and Art Gallery, Bristol, U.K.; **MB.R.**, Museum für Naturkunde, Berlin, Germany; **MCP**, Museu de Ciências e Tecnologia, PUCRS, Porto Alegre, Brazil; **LPRP/USP**, Laboratório de Paleontologia de Ribeirão Preto, Universidade de São Paulo, Ribeirão Preto, Brazil; **NMMNHS**, New Mexico Museum of Natural History & Science, Albuquerque, U.S.A; **NMT**, National Museum of Tanzania, Dar es Salaam, Tanzania; **PULR**, Universidad Nacional de La Rioja, La Rioja, Argentina; **PVL**, Fundación Miguel Lillo, Tucumán, Argentina; **PVSJ**, Museo de Ciencias Naturales, San Juan, Argentina; **QG**, Natural History Museum of Zimbabwe, Bulawayo, Zimbabwe; **SAM-PK**, Iziko South African Museum, Cape Town, South Africa; **SMNS**, Staatliches Museum für Naturkunde, Stuttgart, Germany; **ULBRA**, Museu de Ciências Naturais, Universidade Luterana do Brasil, Canoas, Brazil.

GEOLOGICAL SETTING

The new specimen comes from deposits of the Alemoa Member of the Santa Maria Formation, at the site known as Waldsanga (Figure 1; Huene, 1942; Langer, 2005b; Langer et al., 2007) or Cerro da Alemoa (Da Rosa, 2004, 2015). The same site has also yielded the type specimens of the early sauropodomorph *Saturnalia tupiniquim* (Langer et al., 1999), the rauisuchian *Rauisuchus tiradentes* (Huene, 1942), and the cynodonts *Gomphodontosuchus brasiliensis* (Huene, 1928; Langer 2005a) and *Alemoatherium huebneri* (Martinelli et al., 2017). However, the most common fossils recovered from the site are rhynchosaurs of the genus *Hyperodapedon* (Langer et al., 2007)

Reddish, massive mudstones of the Alemoa Member compose the main lithology of the site, in contact with the yellowish to orange stratified sandstones of the overlying Caturrita Formation. The fine-grained beds of the Alemoa Member correspond to floodplain deposits, and are subdivided into lower, intermediate, and upper levels, whereas the coarser deposits of the Caturrita Formation represent ephemeral, high-energy channel and crevasse-splay deposits (Da Rosa, 2005, 2015). The lower and intermediate levels of the exposed Alemoa Member represent distal floodplain deposits, whereas the upper level represents a proximal floodplain (Da Rosa, 2005, 2015).

According to recent sequence stratigraphy studies (Horn et al., 2014), the strata exposed at the site belong to the Candelária Sequence, Santa Maria Supersequence (Santa Maria 2 Sequence of Zerfass et al., 2003), which includes the upper part of the Santa Maria Formation (Gordon, 1947) and the lower part of the Caturrita Formation

(Andreis et al., 1980). Two assemblage zones (AZ) have been recognized within the Candelária Sequence: the older *Hyperodapedon* AZ and the younger *Riograndia* AZ. The occurrence of *Hyperodapedon* rhynchosaurs justifies correlating the site to the *Hyperodapedon* AZ.

Correlations with radioisotopically dated strata from the Ischigualasto Formation (Ischigualasto–Villa Unión Basin) in western Argentina (e.g., Martínez et al., 2011, 2012) that share a similar faunal association (e.g., Langer, 2005b; Langer et al., 2007) indicate that the *Hyperodapedon* AZ is late Carnian in age. This age is corroborated by detrital radiometric dating of the reddish mudstones at the level from which *Saturnalia tupiniquim* was collected, which has yielded a maximum age of c. 233 Ma (Langer et al., 2018).

SYSTEMATIC PALEONTOLOGY

DINOSAURIFORMES Novas, 1992 sensu Nesbitt, 2011

DINOSAURIA Owen, 1842 sensu Padian and May, 1993

SAURISCHIA Seeley, 1887 sensu Gauthier, 1986

cf. THEROPODA Marsh, 1881 sensu Gauthier, 1986

NHANDUMIRIM WALDSANGAE, gen. et sp. nov.

(Figs. 2–15)

Holotype—LPRP/USP 0651, a partial postcranial skeleton (Fig. 2), consisting of three trunk vertebrae, two sacral vertebrae, seven caudal vertebrae, a chevron, pelvic and hindlimb bones from the right side of the body including an ilium, femur, partial tibia, fibula, metatarsals II and IV, ungual and non-ungual phalanges. The bones were found in close association within an area approximately 50 cm by 50 cm, and were

semi-articulated. Some fragmentary remains are not identifiable due to their incompleteness.

Etymology—The generic name combines the Portuguese derivatives of the indigenous Tupi-Guarani words *Nhandu* (running bird, common rhea) and *Mirim* (small), in reference to the size and inferred cursorial habits of the new dinosaur. The specific epithet name refers to the Waldsanga site, the historical outcrop (Langer, 2005a) that yielded this new species.

Type Locality and Horizon—Site known as Waldsanga (Huene, 1942; Langer et al., 2007) or Cerro da Alemoa (Da Rosa, 2004, 2015), at coordinates 29º41'51.86"S and 53º46'26.56"W, in the urban area of Santa Maria, Rio Grande do Sul State, southern Brazil. The new dinosaur comes from the upper levels of the Alemoa Member of the Santa Maria Formation, 1–1.5 m below the contact with the overlying Caturrita Formation, in the proximal floodplain deposits of the Candelária Sequence of the Santa Maria Supersequence (Zerfass et al., 2003; Horn et al., 2014).

Diagnosis—A saurischian dinosaur distinguished from all other Carnian dinosauromorphs by the following unique combination of autapomorphic characters: sharp longitudinal keels on the ventral surfaces of the proximal caudal centra; brevis fossa projecting for less than three-quarters of the length of the ventral surface of the iliac postacetabular ala; proximally short dorsolateral trochanter that terminates well distal to the level of the femoral head; distal tibia with a mediolaterally extending tuberosity on its cranial surface, in addition to a tabular-shaped caudolateral flange; conspicuous craniomedially oriented semi-circular articular facet on the distal fibula, probably related to the articulation of the lateral face of the ascending process of the astragalus; straight metatarsal IV.

DESCRIPTION

Axial Skeleton

Three caudal trunk vertebrae, two sacral vertebrae, with an isolated sacral rib, seven caudal vertebrae and a chevron have been recovered. For descriptive purposes, the trunk, sacral and caudal vertebrae will be sequentially numbered from the most cranial to the most caudal.

Trunk Vertebrae—Two trunk vertebrae ("1" and "3") are known only from their centra, whereas a third (trunk vertebra "2") also includes a poorly preserved neural arch (Figs. 3, 4). The vertebrae were arbitrarily ordered "1"–"3" based on their length: the longer elements are inferred to be more cranial, and the shorter more caudal. The absence of parapophyses, ventral keels, or chevron facets suggests that all three centra represent caudal trunk elements. The centra are spool-shaped and craniocaudally elongated in comparison with the typically craniocaudally compressed caudal trunk vertebrae of herrerasaurids (Novas, 1994; Bittencourt and Kellner, 2009). Their lateral surfaces have a craniocaudally oriented shallow depression, which is pierced by small nutrient foramina. The length:height ratios of vertebrae "1" to "3" rounds 1.4. Their articular faces are gently concave and rounded, but slightly taller than wide. Although the centra cannot be precisely oriented due to the absence of anatomical landmarks, the surface that we tentatively identify as the cranial articular surface of trunk vertebra "1" is notably shorter dorsoventrally than is the caudal articular surface.

Part of the neural arch is preserved in trunk vertebra "2" (Figs. 3B, 4). The prezygapophysis is short, not projecting beyond the cranial edge of the centrum. In cranial view, the articular surface of the prezygapophysis faces dorsomedially and articulates with the postzygapophysis at an angle of about 35 degrees to the horizontal.

The prezygodiapophyseal lamina reaches the prezygapophysis. Only a small part of the left transverse process is preserved, and it projects dorsolaterally. The caudal part of the left side of the neural arch preserves a well-developed fossa (the caudal chonos or postzygapophyseal centrodiapophyseal fossa of Wilson et al., 2011). This fossa is cranially bounded by a nearly vertical posterior centrodiapophyseal lamina (Wilson et al., 1999) so that the postzygapophyseal centrodiapophyseal fossa is only visible in lateral and caudal aspects. Cranial to this lamina, the badly preserved caudal portion of the medial chonos (or centrodiapophyseal fossa of Wilson et al., 2011) is visible. The postzygodiapophyseal lamina forms the dorsomedial border of the postzygapophyseal centrodiapophyseal fossa and contacts the posterior centrodiapophyseal lamina in its dorsalmost extension. The confluence between the left caudal pedicel of the neural arch and the roof of the neural canal forms the ventral margin of the postzygapophyseal centrodiapophyseal fossa. Postzygapophyses and possible hyposphene-hypantrum articulations are not preserved in the preserved trunk vertebrae.

Sacral Vertebrae—The recovered parts of the sacrum (Fig. 5) include an isolated and badly preserved centrum, the second primordial sacral vertebra still attached to its right rib, and an isolated left rib from the first primordial sacral vertebra. No remains of the neural arches were identified. Both preserved centra are craniocaudally short and robust. The isolated centrum is as long as wide, whereas that of the second sacral vertebra is slightly longer than wide. The ventral surfaces of the centra are less strongly concave in lateral view than those of the trunk and proximal caudal vertebrae. The recovered sacral vertebrae are not fused to one another, and there is no evidence for fusion of the sacral ribs with either the vertebra or the ilium. Several tiny nutrient foramina are present on the caudolateral half of the centrum of the second sacral vertebra. The articular surfaces of the centra are weakly concave and wider than

tall. In both sacral centra the cranial articular surface is broader transversely than is the caudal articular surface. The rib is firmly attached (but not fused) to the second sacral centrum, and there is a conspicuous swelling along the caudoventral margin of the articulation surface. The articulation surface with the rib occupies more than half of the craniocaudal length of the centrum. In contrast, in the isolated sacral centrum, the rib articulation surface is restricted to its cranial half.

The partial isolated rib from the first sacral vertebra (Fig. 5F, G) is mediolaterally wider than both recovered sacral centra. Those proportions are due to the iliac and sacral shortening in *Nhandumirin waldsangae* compared to other dinosauromorphs, such as *Saturnalia tupiniquim* (MCP-3845 PV). The rib is slightly concave and fan-shaped in dorsal aspect, being more dorsoventrally flattened along its incomplete cranial margin, whereas the lateral and caudal margins are confluent and form a gently curved profile. In lateral view, the rib has a smooth articular surface for the medial surface of ilium, and its cranial margin curves gently dorsally towards the contact with the transverse process (which is not preserved). This condition differs from the L-shaped cross section of the first sacral rib of *Saturnalia tupiniquim* (Langer, 2003).

The preserved right rib of the second sacral vertebra is missing its caudodorsal and cranioventral tips. The rib expands in dorsoventral height distally from the centrum, and its ventral surface is concave in cranial and caudal views. In dorsal and ventral views, the most cranial tip of the rib extends beyond the cranial limit of the centrum. In lateral view, the articular surface of the sacral rib expands dorsoventrally towards its caudal margin, i.e. it is narrower dorsoventrally at its cranial portion. The articular surface is smooth and slopes from cranioventrally to caudodorsally.

Caudal Vertebrae and Chevron—The seven recovered caudal vertebrae (Figs. 6, 7) are from different parts of the tail. They are generally more complete than those of the trunk and sacral series, preserving at least parts of the neural arch in all recovered elements. Caudal vertebrae “1”–“3” come from the first third of the tail, whereas vertebrae “4”–“5” represent mid-caudal vertebrae, and vertebrae “6”–“7” are distal caudal elements. The neurocentral suture is only visible in the three more proximal vertebrae, suggesting it is completely closed in more distal caudal vertebrae. The lateral surfaces of caudal centra “1”–“4” have shallow, proximodistally oriented, and distally positioned depressions, within each of which there are one or two tiny nutrient foramina. The caudal centra become increasingly elongate towards the distal part of the tail, changing from proximal caudal vertebrae with spool-shaped centra to distal caudal vertebrae with much more elongated centra. The length:height ratio of caudal centrum “1” is 1.0, increasing to 1.3 in caudal vertebrae “2”–“3”; 2 in caudal vertebrae “4”–“5”; and >3 in caudal vertebra “6”. The proximal and distal articular faces are round (caudal vertebrae “1”, “4”–“6”) or oval (caudal vertebrae “2”–“3”) in outline, and have concave surfaces with the proximal articular face always deeper than the distal. The ventral surfaces of caudal vertebrae “1”–“3” bear a craniocaudally extending keel. In caudal vertebra “1”, the keel is conspicuous only on the caudal half of the ventral surface of the centrum, is constricted at its midlength, and is laterally bounded by shallow excavations. The ventral keels of caudal vertebrae “2” and “3” lack the lateral excavations, but are stouter and extend for the whole ventral surface of the centrum.

Facets for chevron articulation are seen in caudal vertebrae “1”–“5”. Only the distal articulation for the chevron is present in caudal vertebra “1”. This suggests that this vertebra would have received the first chevron of the series, and therefore likely represents the first caudal vertebra. In caudal vertebra “1”, the area for the chevron

attachment includes two distinct articular facets. In caudal vertebrae “2”–“5” there are single, larger, continuous, and oval facets for the chevrons on both the proximal and distal articular facets of the centra.

The transverse processes are dorsolaterally directed in all caudal vertebrae. In caudal vertebra “1”–“3’ they are also oriented caudolaterally in dorsal view, whereas in caudal vertebra “4” the transverse process is directed strictly laterally and forms a right angle with the centrum. Except for the cross-sectional morphology (see below), the precise length and shape of the transverse processes cannot be assessed in caudal vertebrae “1”–“3” due to damage. In caudal vertebra “4”, the transverse process is rectangular, and in caudal vertebra “5” it is reduced to a small bump. Transverse processes are absent in caudal vertebrae “6”–“7”. In cross-section, the transverse process is triangular in caudal vertebrae “1”–“2” and blade-like in caudal vertebrae “3”–“4”. The neural spine is best preserved in caudal vertebra “5”. It is parallelogram-shaped and its length is equal to two thirds of the centrum length. Its tip projects further distally than the distal border of the centrum. A preserved neural spine fragment of caudal vertebra “3” suggests that it is distally inclined.

The articular surfaces of the prezygapophyses face dorsomedially, whereas those of the postzygapophyses face ventrolaterally. The pre- and postzygapophyses articulate with one another at an angle of about 60° to the horizontal, except in caudal vertebra “1”, where the articulation is at 40° to the horizontal. The zygapophyseal articular surfaces of the caudal vertebrae are always set close to the vertebral body. Caudal vertebra “6” has stouter prezygapophyses than the preceding vertebrae, but they do not extend proximally far beyond the cranial centrum rim. Hyposphene-hypantra articulations are not present in the caudal vertebrae.

Two laminae are present on the neural arches of caudal vertebrae “1”–“4”. A faint prezygo-postzygopophyseal lamina (Ezcurra, 2010) extends along the dorsal surfaces of the neural arches of caudal vertebrae “3” and “4”, but does not reach either the pre- or the postzygapophyses. A more conspicuous lamina is present in caudal vertebrae “1”–“4”, in a similar position to the prezygodiapophyseal lamina of trunk vertebrae. In tail vertebrae “1”–“2”, this lamina forms the craniodorsal margin of a shallow concave surface, here interpreted as the prezygapophyseal parapodiapophyseal fossa (Wilson et al., 2011).

The only preserved chevron is isolated (Fig. 7G, H) and its position in the caudal column is uncertain. Its distal tip is missing, and the lateral edges of the proximal articulation are not preserved. The proximal articular surface is saddle-shaped and notably concave in cranial and caudal views. Cranially, the shaft has a subtle proximodistally extending sulcus near its proximal articulation, whereas in caudal view, the sulcus extends further distally and is deeper than its cranial counterpart. These sulci mark the openings for the haemal canal, but the exact shape of this canal cannot be described because the sulci are filled with matrix. The distal part of the chevron shaft is inclined caudally at 40° to the vertical in lateral view, and becomes mediolaterally narrower towards its distal end.

Appendicular Skeleton

Ilium—The ilium is incomplete (Fig. 8), lacking most of the dorsal lamina above the acetabulum, the caudal tip of the postacetabular ala, the cranial extension of the supraacetabular crest, and the lateroventral portion of the pubic peduncle.

The preacetabular ala does not extend cranially as far as the cranial edge of the pubic peduncle. The ala is subtriangular in lateral view, cranially directed, with a gently

rounded tip and a cranioventral margin that forms an angle of 80° with the dorsal margin. In dorsal view, the preacetabular ala arches laterally as it extends cranially. The angle formed by the pre- and postacetabular alae suggests that the iliac lamina was laterally concave, as seen in other dinosauriforms (Sereno and Arcucci, 1994; Novas, 1994; Langer, 2003; Martínez and Alcober, 2009). Muscle scars are present on the dorsal rim of the lateral surface of the preacetabular ala, and represent the insertion of the M. iliotibialis (Hutchinson, 2001a). The embayment between the preacetabular ala and the iliac body is cranially excavated by a dorsoventrally oriented and shallow preacetabular fossa (Hutchinson, 2001a; Langer et al., 2010b).

The dorsal margin of the supraacetabular crest is positioned at 47% of the dorsoventral height of the ilium and covers most of the craniocaudal extent of the acetabulum. The crest gently projects ventrolaterally, and the mediolaterally broadest point of the crest is located directly above the midpoint of the acetabulum. The ventral margin of the ilium is concave, indicating a perforated acetabulum. On the caudoventral portion of the acetabulum, the acetabular antitrochanter has a roughly squared outline, with several conspicuous, but low scars. The pubic peduncle has a cranioventrally facing articulation for the pubis. The ischiadic peduncle is columnar, with its caudodorsal and medial surfaces slightly flattened. It projects caudoventrally, with a concave caudal margin. The caudoventrally facing articular surface for the ischium is flat, rugose and suboval in outline and gently laterally deflected.

Two foramina pierce the ventrolateral margin of the ilium, at the cranial margin of the postacetabular ala. Caudal to these openings, a well-developed, but craniocaudally short brevis fossa occupies less than three-quarters of the length of the ventral margin of the postacetabular ala. The postacetabular ala is longer than the space between the pre- and postacetabular embayments. The ventrally oriented lateral wall of

the brevis fossa originates well caudal to both the supraacetabular crest and the ischiadic peduncle, whereas the medial wall of the brevis fossa expands medioventrally. The internal surface of the brevis fossa is rugose, and corresponds to the attachment area for the M. caudofemoralis brevis (Gatesy, 1990).

The dorsal lamina of the postacetabular ala is mediolaterally thin when compared to those of other Triassic dinosaurs (e.g., *Coelophysis bauri*, AMNH FARB 2708; *Saturnalia tupiniquim*, MCP 3845-PV; Langer et al., 2011b), and the same condition is observed for the dorsal lamina of the preacetabular ala. The entire lateral surface of the postacetabular ala is covered with muscle scars, which are caudal extensions of the scars present on the lateral surface of the pretacetabular ala, and which are related to the insertion of M. iliotibialis (Hutchinson, 2001a; Langer, 2003; Langer, et al., 2010b).

The medial surface of the ilium bears a complex set of scars, including those for the sacral rib attachments. The scar of the first primordial sacral rib is rounded and L-shaped, with its apex pointing cranioventrally. Cranially, this scar nearly reaches the medial margin of the preacetabular fossa, but it is placed caudal to the base of the pubic peduncle. Its ventral margin parallels the ventral rim of the brevis fossa, and is continuous backwards to a point where it converges with the medial wall of that fossa. Along all its extension, this scar is slightly dorsally bowed, without any clear distinction of the articulation facets for the ribs of sacral vertebrae 2 and 3. Nevertheless, we presume that there were three sacral vertebrae in *Nhandumirim waldsangae*. This is based on the 4.6 cm length of the scars for the articulation of the sacral vertebrae on the ilium, whereas the total length of the two preserved sacral centra (1.5 and 1.4 cm, respectively) covers less than 65% of this length. Accordingly, the remaining space

would receive a third sacral vertebra, as seen in *Saturnalia tupiniquim* (MCP-3845 PV) (see Discussion).

Femur—The femur is nearly complete (Fig. 9) and slightly longer than twice the craniocaudal length of the ilium. At midshaft, the femur is subcircular in cross section, with a diameter of 1–1.2 cm. The bone wall thickness is approximately 20% of the femoral diameter, as measured on the cranial margin of the bone at the level of the distal end of the fourth trochanter. In addition to the thin bone wall, the femur is also remarkably slender: 12 cm long and 3.5 cm in circumference at midshaft (ratio = 3.4). Other early dinosaurs are more robust, such as *Saturnalia tupiniquim* (MCP 3844-PV), which has a femur that is 15 cm long and a midshaft circumference of 5 cm (ratio = 3). However, such differences would possibly be explained by allometric growth.

The femur is sigmoidal, particularly in cranial and caudal views, due to the cranial and medial bowing of the shaft and the inturned head. The femoral head is about one third wider mediolaterally than the femoral "neck" in cranial and caudal views, and more than twice mediolaterally longer than craniocaudally broad in proximal view. It is rugose and bears a distinct straight proximal groove which gently curves medially in its cranial extent and extends caudolaterally from the cranial margin of the head. Another faint and nearly mediolaterally extending ridge marks the cranial limit of the distally descending facies articularis antitrochanterica. The elevated caudal corner of the femoral head, or "greater trochanter", forms a nearly right angle in caudal view. The medial tuber is well developed and rounded, occupying one third of the medial edge of the femoral head. Its caudal rim continues laterally as the ridge extending over the cranial margin of the facies articularis antitrochanterica. A medial ridge extends distally from the medial tuber. The medial tuber is separated from the craniomedial tuber by the concave and scarred ligament sulcus. This scarred area extends proximodistally parallel

to the medial ridge, and merges with a larger set of scars that surrounds the proximal portion of the fourth trochanter. The medial ridge is smooth, and caudally bounded by a shallow and somewhat concave surface distal to the fossa articularis antitrochanterica. This surface bears some roughly rounded small scars, and is caudodistally bounded by another proximodistally smooth ridge (Fig. 9C:‘oi’) that fades into the proximal slope of the fourth trochanter. This ridge possibly represents the insertion of the M. obturatorius (Langer, 2003).

The craniomedial tuber is well developed, rounded, medially projected, and larger than the medial tuber. Lateral to it, a small and rounded caudolateral tuber is present. The craniomedial tuber is distally bounded by a saddle-shaped notch that extends laterodistally, delimiting the scarred ventral emargination. Its scars merge medially with those of the ligament sulcus. The craniomedial surface of the femoral head (Langer and Ferigolo, 2013) bears muscle attachment scars, and is marked caudally by a sharp craniomedial crest (Bittencourt and Kellner, 2009). This crest extends distally from the craniolateral tuber, and fades away at the level of the cranial trochanter. An extensive, scarred flat surface is present along the whole lateral surface of the proximal end of the femur lateral to the aforementioned ridge. These scars are probably related to the dorsolateral ossification (sensu Piechowski et al., 2014) and the anterolateral scar (sensu Griffin and Nesbitt, 2016a). Although no clear association to any specific muscle insertion has been established, these scars may be related to the iliofemoral ligament (Griffin and Nesbitt, 2016a).

The cranial trochanter is a proximodistally oriented ridge that becomes distally broader, and then merges into the shaft at the level of the cranial limit of the fourth trochanter. The dorsolateral trochanter is a faint, proximodistally elongated ridge, which does not continue proximally to the level of the femoral head. It is essentially “short”, as

is the cranial trochanter. Muscles scars surround both trochanters, and although the trochanteric shelf is not present, these scars probably represent the attachment of M. iliofemoralis externus (see Hutchinson, 2001b). In cranial view, a smooth linea intermuscularis cranialis extends distally from the medial margin of the cranial trochanter, reaching the distal third of the shaft. In birds, this intermuscular line forms the border between M. femorotibialis medialis/M. femorotibialis intermedius and M. femorotibialis externus (Hutchinson, 2001b).

The fourth trochanter is set on the medial half of the shaft. It is a well-developed, rugose, and sinuous flange for the attachment of M. caudofemoralis longus (see Hutchinson, 2001b). Its proximal portion forms a low angle with the shaft, and has a sinuous outline in caudal view. It merges distally with the shaft, forming a steeper angle. Medial to the fourth trochanter, there is an oval depression, or fossa, that is also for insertion of M. caudofemoralis longus (Hutchinson, 2001b; Langer, 2003). The scar for the attachment of M. caudofemoralis brevis (Hutchinson, 2001b; Griffin and Nesbitt, 2016a) is rounded and proximolaterally located relative to the fourth trochanter.

The shaft of the distal third of the femur expands transversely and caudally. Along this portion of the bone, two longitudinally oriented intermuscular lines, the caudomedial and caudolateral lines (“fcmil” and “fclil” of Langer, 2003, respectively), form the borders of the distal femur. Between them, there is a well-developed, U-shaped popliteal fossa, bordered by low lateral and medial walls. In birds, the popliteal fossa corresponds to attachment of the M. flexor cruris lateralis pars accessorius (Hutchinson, 2001b). In cranial view, the distal quarter of the femur is straight and shows a distinct muscle scar on its laterocranial portion (“fdms” of Langer, 2003), as well as a set of scars that extend proximally from the distal margin of the femur, fading proximomedially at the level of the aforementioned scar. These two scarring areas may

correspond to the “unusual subcircular muscle scar” of *Herrerasaurus ischigualastensis* (Novas, 1994:406), later referred to as the craniomedial distal crest by Hutchinson (2001b).

The distal condyles are not well preserved and are offset medially due to a breakage. They are rugose and form a distal outline that is wider lateromedially than craniocaudally. The medial condyle comprises the whole medial half of the distal part of the femur, and is twice as long craniocaudally as it is wide. It is medially rounded, with a subtle caudal extension. In distal view, the medial condyle has a squared caudomedial corner, whereas the craniomedial and the caudolateral corners are rounded and separated from the lateral condyle by the sulcus intercondylaris. The sulcus intercondylaris extends craniocaudally for at least one third of the length of the medial condyle. Lateral to it, only a small and relatively uninformative portion of the lateral condyle is preserved. Although damaged, the crista tibiofibularis seems to be rounded, somewhat caudally expanded, and laterally directed. In addition, the crista tibiofibularis is separated from the lateral condyle by a smooth and concave surface in distal view, which extends proximally for about half of the length of the popliteal fossa.

Tibia—The bone is incomplete (Figs. 10, 11), crushed and missing its proximal quarter. The shaft is rod-like and circular in cross-section at midlength. The distal end is mediolaterally expanded and the articular surface is rugose. In distal view, the tibia is trapezoidal, with rounded corners and the cranial margin lateromedially broader than the caudal. In cranial view, a subtle mediolaterally expanded anterior diagonal tuberosity (Ezcurra and Brusatte, 2011; Nesbitt and Ezcurra, 2015) is visible. This tuberosity is closer to the medial corner, and exposed in medial, lateral, and distal views as a low lump. In lateral view, a proximodistally oriented groove extends proximally for about 10 mm. In distal view, this groove excavates laterally the tibia for about 20% of its

mediolateral width. The tibial facet for the ascending process of the astragalus is positioned cranial to the caudolateral flange. It is a well-developed surface, occupying half of the distal surface of the tibia. This facet forms an angle of about 25˚ with the distal margin of the tibia, suggesting that it would have articulated with a high and well-developed ascending process of the astragalus. The caudolateral flange of the tibia is tabular (Nesbitt and Ezcurra, 2015), but does not extend beyond the lateral limit of the cranial part of bone. Its mediolateral border bears a small mound-shaped projection that faces distally, which increases the distal extension of the bone. The tibia has a flat caudal surface, bearing medially a faint and proximodistally oriented ridge. Its caudomedial corner has a shallow notch that receives the caudomedial process of the astragalus. This notch has a rounded aspect in caudal and lateral views. In distal view, it fades laterally before the separation between the caudolateral flange and the facet for the astragalar ascending process.

Fibula—The fibula is more complete than tibia (Figs. 10, 11), albeit also crushed and lacking part of the cortical bone. It is nearly 10% longer than the femur, indicating that the epipodium was longer than the propodium in *Nhandumirim waldsangae*. Its proximal end is rugose and mediolaterally compressed, being three times longer craniocaudally than wide mediolaterally. The proximal end of the fibula is somewhat medially bowed, caudally expanded, and more than twice as wide as the shaft. In medial view, the first third of the fibula has a proximodistally-oriented scar for attachment of the M. iliofibularis (Langer, 2003) (Fig. 10C), which extends to the cranial surface of the bone, where it fades out. The proximal third of the lateral surface of the fibula is also scarred, and two small foramina are found on the medial surface of the bone near the midshaft. The shaft is straight and slender, and “D”-shaped in cross-section at midshaft, with a flatter medial surface.

The articular surface of the distal end of the fibula is rugose and flattened, forming a right angle to the long axis of the bone in lateral and medial views. The distal end is slightly mediolaterally expanded, whereas the craniocaudal length is twice that of the bone shaft. The cranial margin of the distal end is flat and nearly parallel to the shaft, whereas the caudal margin is caudally expanded. Scars are present on the medial side of the distal end of the fibula, and they may represent a ligamentous attachment to the tibia, as inferred for *Saturnalia tupiniquim* (Langer, 2003). The distal portion of the fibula also shows a distinct facet that occupies the cranial half of its medial side. This conspicuous facet extends proximally and has a semicircular shape both in medial and distal views. It probably articulated with the lateral face of the ascending process of the astragalus. In lateral view, the distal portion of the fibula is scarred for muscle insertion, and the bone surface is rugose and has an overall elliptical shape in distal view.

Pes—Only metatarsals II and IV of *Nhandumirim waldsangae* are preserved (Fig. 12). Although compressed in its proximal half, the length of metatarsal II indicates that the metapodium of *Nhandumirim waldsangae* is longer than half of the length of the propodium and epipodium.

The proximal end of metatarsal II is craniocaudally flattened. In proximal view, the long axis of the proximal end is rotated by about 20˚, so that it is craniolaterally to caudomedially oriented. The proximal articular surface is planar, mediolaterally expanded, with nearly squared corners in proximal view. The craniomedial and caudolateral faces, for contact with metatarsals I and III, respectively, are flat and scarred. The shaft of metatarsal II is straight, and progressively expands lateromedially towards the distal end to form the distal condyles. The distal condyles have well-developed ligament pits, with the lateral deeper than the medial. Proximal to the ligament pits, the cranial surface of the metatarsal bears a raised surface, which has

conspicuous scars for ligamentous insertion and is best developed at the craniolateral margin of the bone. The lateral and medial distal condyles are subequal in length, but the former is more distally expanded than the latter. In distal view, the articular facet for the first phalanx is asymmetric: the cranial and lateral faces are flattened, whereas the caudal and medial surfaces are slightly concave, forming an angled caudomedial corner.

The proximal quarter of metatarsal IV is damaged. However, the bone was probably subequal in length to metatarsal II because, in medial and lateral views, the proximal part of the shaft has the proximal scars for articulation with metatarsals III and V. Metatarsal IV is straight, and its distal end also shows scars for ligament insertions. In distal view, its cranial face is somewhat convex, whereas the other surfaces are concave, with the corners forming acute angles. The caudolateral corner is drawn out into a subtriangular process in distal view. The condyles are asymmetrical, being craniocaudally longer than lateromedially wide. A shallow and mediolaterally oriented furrow is set caudal to the condyles and cranial to the caudolateral corner of the metatarsal II.

The pedal digits are represented by five non-ungual and three ungual phalanges (Fig. 13). However, as these elements were not preserved in articulation, both their position in the foot, and the phalangeal formula for *Nhandumirim waldsangae,* is uncertain.

One of the non-ungual phalanges, referred to as phalanx A (Fig. 13), is mediolaterally broader than the other preserved phalanges, and probably represents a first phalanx, as the outline of its proximal articulation is wider than high. In addition, the small dorsal intercondylar process suggests it would have articulated with a metatarsal. The other non-ungual phalanges have a proximal articulation that is about as high as wide, with a vertical ridge that separates the concave articular surface into

medial and lateral facets. This ridge is also present, but fainter, in phalanx A. In all non-ungual phalanges, the proximal half of the plantar surface is flattened and scarred for the insertion of the collateral and flexor ligaments. There are well-developed dorsal intercondylar processes. The process is not as well developed in phalanx A, which also bears fainter scars related to the insertion of the extensor ligaments.

A few foramina are seen on the shafts of the phalanges. A plantar-dorsal constriction is present in the distal half of the shaft, and forms a neck just proximal to the well-developed distal condyles. Pits for collateral ligaments are present on the lateral and medial margins of the distal condyles, and shallow pits for the extensor ligaments are also present. The distal articulation is ginglymoid, with separated condyles, although there is variation in shape. The articular surfaces of phalanges A and D are wider than high, whereas the articular surfaces of phalanges B and C (the distal condyles are missing in phalanx E) are nearly as wide as high.

The ungual phalanges have proximal articular surfaces that are higher than wide, also bearing a vertical ridge that separates medial and lateral articular facets. The dorsal intercondylar process is smaller than in the non-ungual phalanges, but its dorsal margin bears more clearly marked scars for the extensor ligaments. The flexor tubercles are well developed and mound like. The ungual phalanges are subtriangular in cross-section at midlength. They are curved, with their tips projected well beneath the base of the proximal articulation, but not as raptorial as in later theropods (see Rauhut, 2003). Attachment grooves for the ungual sheath are also present in both the medial and lateral sides of the unguals.

Osteohistology

Bone samples from the tibia and fibula (Fig. 14-15) were taken as close to the midshaft as possible, because this area preserves a larger amount of cortical tissue and growth marks (Francillon-Vieillot et al., 1990; Andrade and Sayão, 2014). The bones were measured, photographed and described for bone microstructure investigation before being sectioned, according to the methodology by Lamm (2013). The bone samples for histological slide preparation were taken from ca. 1cm thick wafers. The sectioned samples were immersed in clear epoxy resin Resapol T-208 catalyzed with Butanox M50. They were cut with the aid of a micro rectify (Dremel 4000 with extender cable 225) coupled to a diamond disk, after they were left to dry. Then, the section assembly side was ground and polished in a metal polishing machine (AROPOL-E, AROTEC LTDA) using AROTEC abrasive grit (grit size 60 / P60, 120 / P120, 320 / P400, 1200 / P2500) to thin the block and remove scratches. After polishing, the blocks were glued on glass slides and thinned again, in order to make them translucent enough for observation of osteohistological structures through light microscopy. All sections were examined and photographed in a light microscope (Zeiss Inc. Barcelona, Spain) equipped with an AxioCam camera with Axio Imager, after the histological slides were prepared. The M2 imaging software was used in the examination procedure.

The osteohistological terminology follows Francillon-Vieillot et al. (1990), except for the definition of laminar bone, for which we follow Stein and Prondvai (2014). General features of the cross-section are described from the endosteal margin to the periosteal surface.

Tibia—The compact cortex of the tibia is composed of laminar bone (Fig. 14), which occurs in long bones of several extinct and extant vertebrate groups (see Stein and Prondvai, 2014). The low variation of lamina density and thickness observed here is

consistent with principles of laminar bone (Hoffman et al., 2014). The vascular network has a homogeneous pattern for the entire transverse plane of the bone (Fig. 14C). It is composed of anastomosed vascular canals in a plexiform arrangement (Fig. 14E).

The medullary cavity and the inner portion of the cortex lack trabecular bone, differing from the pattern observed in *Silesaurus opolensis* in which the perimedullary region shows cancellous bone forming trabeculae (Fostowicz-Frelik and Sulej, 2010). In the inner cortex, the vascular canals extend all the way to the medullary cavity, with no deposition of inner circumferential lamellae. In this area the remodelling process is incipient, indicating the beginning of the resorption process, marked by few erosion rooms and two primary osteons (Fig. 14D). The middle cortex exhibits two lines of arrested growth (LAGs), although no other growth marks as annuli or zones are present. Growth marks are rare and generally appear later in ontogeny in sauropods (see Sander et al., 2011). This is the contrary condition of early sauropodomorphs in which they have been recorded as annuli in *Plateosaurus engelhardti* (Sander and Klein, 2005; Klein and Sander, 2007), growth marks in *Massospondylus carinatus* (Chinsamy, 1993), and LAGs in *Thecodontosaurus antiquus* (de Riqclès et al., 2008, Cherry, 2002). Also, in other dinosauriforms, like *Silesaurus opolensis*, growth marks are broadly spread in different bones as annuli in the femur and tibia, and LAGs in the tibia (Fostowicz-Frelik and Sulej, 2010). The presence of two LAGs in *Nhandumirim waldsangae* shows two interruptions in its bone deposition, indicating two growth cycles at the moment of its death. The outer cortex presents the same pattern as the inner, with the vascular canals extending in the direction of the bone surface. There is no deposition of external lamellae, meaning that an external fundamental system is absent.

The observed pattern is consistent with primary tissues, represented by the plexiform arrangement of the vascular network. The bone deposition was rapid due to the presence of lamellar tissue and the plexiform vascular pattern, a common feature in dinosaurs and birds (e.g. Klein et al., 2012). This tissue is characterized by the interlaced presence of longitudinal, radial, and circular vascular channels (Lamm et al., 2013). The plexiform arrangement is common in sauropod dinosaurs, but not in Triassic sauropodomorphs (Stein and Prondvai, 2014). Due to this feature, the absence of internal and external lamellae and the beginning of bone remodelling, the holotype of *Nhandumirim waldsangae* represents an individual less advanced in ontogeny than reported for *Saturnalia tupiniquim* (paratype MCPV 3846; Stein, 2010) and *Asilisaurus kongwe* (Griffin & Nesbitt, 2016a). In *S. tupiniquim*, the bone has signs of remodelling marked by the presence of secondary osteons, in addition to two LAGs (Stein, 2010), similar to the condition in *N. waldsangae*. The deposition of internal circumferential lamellae on one part of the lamina may also be seen, indicating that MCPV 3846 is more advanced in ontogeny than the only specimen of *N. waldsangae*. As for *A. kongwe*, the main difference is the vascular pattern, which consists of longitudinal primary osteons surrounded by either parallel-fibered or woven bone, with the presence of an avascular region composed of parallel-fibered bone (Griffin & Nesbitt, 2016a). In *N. waldsangae*, longitudinal primary osteons with few anastomoses are present and restricted to the outer cortex. In addition, the presence of lamellae in *S. tupiniquim* indicates that the bone tissue of this taxon already records a decrease in deposition rate, consistent with bone maturity, whereas *A. kongwe* would be less advanced in its ontogeny, although already with signs of decreases in the rate of bone deposition. This differs from the condition presented *N. waldsangae*, indicating that this latter specimen was still growing rapidly at the time of its death, despite the presence of LAGs. This

evidence confirms that the high growth rates observed in Jurassic and Cretaceous dinosaurs (Curry, 1999; Horner et al., 2000, 2001; Sander, 1999, 2000; Erickson and Tumanova, 2000; Sander and Tückmantel, 2003; Sander et al., 2004; Erickson, 2005) were already present in dinosaurs during the Triassic.

Fibula—The bone exhibits the same osteohistological pattern as the tibia (Fig. 15). The beginning of bone remodelling is observed in the perimedular region, with the formation of erosions rooms and a few secondary osteons (Fig. 15C-D). The vascularization is somewhat lower in the endosteal region, with more radial canals, fewer anastomoses. The radial canals are more common between the medial and periosteal regions. In the middle cortex, two lines of arrested growth are present (Fig. 15C), in position and numbers consistent with those present in the tibia. The vascular canals reach the external surface of the periosteal region without the formation of periosteal lamellae (i.e. an external fundamental system is absent).

The osteohistological pattern of *Nhandumirim waldsangae* differs from that of the fibula of *Asilisaurus kongwe*, which is composed mostly by coarse cancellous bone surrounded by a thin cortex of more compact bone (Griffin and Nesbitt, 2016a). Despite the presence of two LAGs in *N. waldsangae*, those differ from the unusual banded pattern of the outer cortex of the fibula in *A. kongwe* fibula. As no other fibula has yet been sampled among early dinosaurs, osteohistological patterns of this bone remain uncertain.

Comparatively, the general osteohistological features of *Nhandumirim waldsangae* are more similar with those of *Silesaurus opolensis*, with some distinctions most related to ontogeny. Both *N. waldsangae* and *S. opolensis* present lamellar bone as the main osteohistological feature (Fostowicz-Frelik and Sulej, 2010), differing from the coarse cancellous bone with a thin compacted bone cortex of *Asilisaurus kongwe*

(Griffin and Nesbitt, 2016a), and the predominantly parallel-fibered bone of Ntaware Formation silesaurids (Peecook et al., 2017). LAGs are present in bones of the largest specimens of *S. opolensis* (Fostowicz-Frelik and Sulej, 2010), in both tibia and fibula of *N. waldsangae*, and absent in Ntaware Formation silesaurids femora (Peecook et al., 2017) and in *A. kongwe*, which have a banded pattern, not associated with growth marks (Griffin and Nesbitt, 2016a). Regarding the osteological maturity of *N. waldsangae*, *S. opolensis* and *A. kongwe*, the most remarkable difference between them is the presence of inner and outer circumferential lamellae in *S. opolensis* (Fostowicz-Frelik and Sulej, 2010), which is absent in the other two. This suggests that the larger specimen of *S. opolensis* was ontogenetically more mature than the *N. waldsangae* and *A. kongwe*. This evidence can be reinforced by the reduction of vascular channels and the absence of anastomoses in *S. opolensis*, whereas it is present in *N. waldsangae*.

DISCUSSION

Comments on the Diagnosis of *Nhandumirim waldsangae*

Despite its incompleteness, the holotype of *Nhandumirim waldsangae* has potential autapomorphies, as well as a unique combination of characters that distinguishes it from other Triassic dinosauromorphs, supporting the recognition of a new genus and species for this specimen.

Regarding its vertebral column, *Nhandumirim waldsangae* has a sacrum comprising three vertebrae. Among early dinosaurs, the presence of three or more sacral vertebrae is plesiomorphic, but the homology of these elements to the primordial pair of sacral vertebrae has been the subject of extensive debate (e.g., Langer and Benton, 2006; Pol et al., 2011; Nesbitt, 2011). One of the paratypes of *Saturnalia tupiniquim*

(MCP 3845-PV) preserves a complete sacral series (Fig. 16), in which a trunk vertebra has been incorporated into the sacrum, and the first primordial sacral attaches caudal to the preacetabular ala of the ilium, medial to the caudal half of the iliac acetabulum. By comparison, the ilium of *Nhandumirim waldsangae* shows that the sacral rib of the first primordial sacral articulated with the ilium immediately caudal to the embayment between the preacetabular ala and pubic peduncle (Fig. 8E, F). This makes it unlikely that a trunk vertebra had been incorporated in the sacrum of *Nhandumirim waldsangae*. It is, however, unclear if the additional sacral vertebra in this latter species corresponds to the insertion of an element between the primordial pair (Nesbitt, 2011) or the incorporation of a caudal vertebra.

The ventral surfaces of the proximal caudal vertebrae in dinosauromorphs are plesiomorphically devoid of marked ornamentations. An exception is *Marasuchus lilloensis* (PVL 3871), the caudal vertebrae of which each bear a ventral longitudinal sulcus (Langer et al., 2013), resembling the condition in neotheropods such as *Dilophosaurus wetherilli* and "*Syntarsus*" *kayentakatae* (Tykoski, 2005). In addition, the proximal caudal vertebrae of the neotheropod *Dracoraptor hanigani* (Martill et al., 2016) bear subtle paired ventral keels. Among Triassic sauropodomorphs, the midcaudal vertebrae of *Panphagia protos* (PVSJ 874) and *Thecodontosaurus antiquus* (BRSMG Ca 7473) possess a shallow and broad ventral sulcus, as also seen in other dinosaur remains with uncertain affinities from the Carnian of south Brazil (Pretto et al., 2015). The proximal caudal vertebrae of *Efraasia minor* (SMNS 12667) resemble the first caudal vertebra of *Nhandumirim waldsangae* in having a ventral keel and lateral excavations, but these are restricted to the distal third of the centra, and more distal vertebrae seem to lack such keels. Accordingly, a ventral keel extending along the entire

length of the centrum of the proximal caudal vertebrae seems to be autapomorphic for *Nhandumirim waldsangae*.

Distal tail vertebrae with short zygapophyses, as seen in *Nhandumirim waldsangae*, are common among non-theropod dinosauromorphs, including the putative theropod *Eodromaeus murphi*. By contrast, in herrerasaurids and neotheropods, the zygapophyses are elongated (Rauhut, 2003; Tykoski, 2005).

The ilium of *Nhandumirim waldsangae* has a perforated acetabulum, a feature that is broadly acknowledged as a synapomorphy of Dinosauria (Brusatte et al., 2010; Langer et al., 2010a; Nesbitt, 2011). In addition, its iliac acetabulum (Fig. 17F) is deeper than in most early sauropodomorphs, such as *Panphagia protos* and *Saturnalia tupiniquim*, and is more similar to the condition in non-dinosaurian dinosauromorphs (Fig. 17A, B). Indeed, the earliest sauropodomorphs differ from *Nhandumirim waldsangae* in having an iliac acetabulum that is much shallower, being about twice as long craniocaudally as deep dorsoventrally (Fig. 17G), measured as the dorsoventral depth from the acetabular roof to the pubis-ischium contact.

Nhandumirim waldsangae has a well-developed brevis fossa on the iliac postacetabular ala, a feature that was hypothesized by Novas (1996) as a dinosaurian synapomorphy. However, recent discoveries revealed a more complex distribution of this feature among dinosauriforms. As pointed out by several authors (Fraser et al., 2002; Langer and Benton, 2006; Brusatte et al., 2010; Langer et al., 2010a; Nesbitt, 2011), a ventrally developed fossa is present in *Silesaurus opolensis*, whereas herrerasaurids, *Tawa hallae*, and a few early ornithischians lack this feature. Although a well-developed brevis fossa cannot be used to nest *Nhandumirim waldsangae* within Dinosauria, the presence of this feature does distinguish it from most non-dinosaurian dinosauromorphs, herrerasaurids, and some other dinosaurs. In saurischians with a well-

developed brevis fossa, the brevis shelf starts cranially as an inconspicuous ridge near to the iliac acetabulum, becoming more prominent along the postacetabular ala (e.g. Langer et al., 2010b). In *Nhandumirim waldsangae*, the ridge does not extend as close to the acetabulum, and the short brevis fossa does not contact the iliac body. This latter feature may represent another potential autapomorphy of the taxon.

The femur of *Nhandumirim waldsangae* differs from those of non-dinosaurian dinosauromorphs, including silesaurids, in possessing a unique combination of features, including: well-developed craniomedial tuber and femoral head; ventrally descending facies articularis antitrochanterica; angled greater trochanter; flanged fourth trochanter; and small crista tibiofibularis (Langer and Benton, 2006; Nesbitt, 2011; Langer et al., 2013).

Nesbitt (2011) discusses the presence of a groove on the proximal surface of the archosaur femur, highlighting that non-dinosaurian dinosauriforms have a deep and straight groove, which is also straight, but faint in sauropodomorphs, whereas it is distinctively curved in early neotheropods. The condition in *Nhandumirim waldsangae* differs from those two. It is deeper and somewhat curved compared to that of sauropodomorphs, but not as curved as in neotheropods. On the other hand, according our first-hand observations, this feature has a more complex distribution among dinosaurs. Whereas some specimens of *Coelophysis bauri* clearly have a distinctive curved groove (e.g. NMMNHS 55344), this is much harder to identify in others (e.g. AMNH FARB 30618). In *Liliensternus liliensterni* (MB.R. 2175) the condition varies, with the left femur bearing a curved proximal groove and the right bone bearing a much straighter groove. Early sauropodomorphs also suggest some degree of variation in this feature. Rather than faint and straight, the proximal groove in one of the paratypes of *Saturnalia tupiniquim* (MCP 3846-PV) is deep and curved, resembling the condition in

N. waldsangae and *Buriolestes schultzi* (ULBRA-PVT280). Accordingly, we prefer to be more conservative and don't assume that *N. waldsangae* bear the neotheropod condition, stressing the need of a more comprehensive discussion of the definition and distribution of this character.

The dorsolateral trochanter of *Nhandumirim waldsangae* is potentially autapomorphic. It is set at the same level as the cranial trochanter, well below the level of the femoral head. Usually in saurischian dinosaurs, the dorsolateral trochanter is positioned well above the level of the cranial trochanter, as seen in *Saturnalia tupiniquim* (Langer, 2003), *Liliensternus liliensterni* (Langer and Benton, 2006; Nesbitt, 2011), and *Staurikosaurus pricei* (Bittencourt and Kellner, 2009). This is also the case in most ornithischians, in which, except in *Eocursor parvus* (see Butler, 2010), the dorsolateral trochanter is closely appressed to the greater trochanter (Norman, 2004; Langer and Benton, 2006).

The distal portion of the hindlimb epipodium of *Nhandumirim waldsangae* bears a unique set of theropod traits, which are uncommon among Carnian dinosauromorphs. In distal view, the tibia differs from those of almost all sauropodomorphs and herrerasaurids in its mediolaterally expanded profile. Early sauropodomorphs, such as *Saturnalia tupiniquim* and *Panphagia protos*, have a distal tibia profile that is nearly as wide transversely as long craniocaudally (Langer, 2003; Martínez and Alcober, 2009), as is also seen in *Eoraptor lunensis* (Sereno, 2012) and *Eodromaeus murphi* (PVSJ 562). *Herrerasaurus ischigualastensis* has a somewhat transversely expanded distal end of the tibia with a rounded cranial margin (Novas, 1994; PVL 2566), and *Staurikosaurus pricei*, and *Sanjuansaurus gordilloi* have a subcircular distal profile (Bittencourt and Kellner, 2009; Alcober and Martínez, 2010). On the contrary, non-heterodontosaurid ornithischians (Butler, 2010; Baron et al., 2017) and neotheropods

(Tykoski, 2005) share with *Nhandumirim waldsangae* a mediolaterally expanded distal end of the tibia.

Nesbitt and Ezcurra (2015) described the caudolateral flange (or posterolateral process) of the neotheropods *Zupaysaurus rougieri*, *Liliensternus liliensterni*, and *Coelophysis bauri* as tabular. A tabular caudolateral flange is more quadrangular than rounded, a shape resulting from a set of deflections. This is similar to the condition in *Nhandumirim waldsangae*, which also resembles neotheropods because it bears the anterior diagonal tuberosity on the cranial surface of the distal end of the tibia (Ezcurra and Brusatte, 2011). Among Carnian dinosauromorphs, the co-occurrence of a tabular caudolateral flange and the anterior diagonal tuberosity has so far been recognized only in the distal end of the tibia of *Nhandumirim waldsangae*.

The astragalus of many neotheropods has a prominent posteromedial process (or caudomedial process), as described for Z*upaysaurus rougieri* (Ezcurra and Novas, 2007). This process fits into a notch in the tibia, seen in the caudomedial corner of the distal surface of the bone. This condition is commonly found in neotheropods, such as "*Syntarsus*" *rhodesiensis* (holotype QG/1), as well as the "Petrified Forest theropod", *Lepidus praecisio*, *Liliensternus liliensterni*, and *Tachiraptor admirabilis* (Padian, 1986; Ezcurra and Novas, 2007; Langer et al., 2014; Nesbitt and Ezcurra, 2015). The caudomedial notch is present in *Nhandumirim waldsangae*, *Eodromaeus murphi* (PVSJ 560, 562), *Guaibasaurus candelariensis* (Langer et al., 2011), and also in some sauropodomorphs, such as *Riojasaurus incertus* (PVL 3845, 4364; Ezcurra and Apaldetti, 2012) and *Coloradisaurus brevis* (Ezcurra and Apaldetti, 2012; Apaldetti et al., 2013).

The fibula of *Nhandumirim waldsangae* has an autapomorphic articular facet on the medial side of its distal end. This facet, which presumably marks the articulation

with the ascending process of the astragalus, was not observed in other early dinosaurs with a non-coossified tibiotarsus. In the fused tibiotarsus of some coelophysoids, the craniomedial corner of the distal fibula forms a flange and overlaps the cranial margin of the ascending process of the astragalus (see Rauhut, 2003; Tykoski, 2005; Ezcurra and Brusatte, 2011). This condition may prove to be homologous with that of *Nhandumirim waldsangae*, but the fusion of elements in coelophysoids hampers the proper evaluation of this feature.

The straight metatarsal IV of *Nhandumirim waldsangae* differs from the sigmoid elements of all well-known early dinosaurs. A similar condition is found in pseudosuchian archosaurs, pterosaurs and in *Lagerpeton chanarensis* and *Marasuchus lilloensis* (Sereno and Arcucci, 1993, 1994; Novas, 1996). Novas (1996) made the observation that metatarsal IV of dinosaurs tends to bow laterally along its distal half. Accordingly, we assume that a straight metatarsal IV represents an autapomorphic reversal of *Nhandumirim waldsangae* among dinosaurs, perhaps related to its small size.

Ontogeny and Taxonomic Validity of *Nhandumirim waldsangae*

The ontogenetic stage of *Nhandumirim waldsangae* is assessed based on (1) the tibia and fibula osteohistology (see above) and (2) the closure of neurocentral sutures. Osteohistology shows unmodified primary tissue as the main structural bony component. Anastomosed vascular canals abound, forming a plexiform arrangement, the beginning of the remodelling process composed by few erosion cavities aside primary osteons in both tibia and fibula and a few and small secondary osteons in the fibula. The medullary cavity and inner portion of the cortex lack trabecular bone and deposition of inner lamellae, as well as the external fundamental system in the outer cortex as well as growth marks like LAGs, annuli or zones. Also, the presence of two

LAGs in the middle cortex suggests that this individual was at least three years old at death. The closure of the neurocentral sutures only in caudal vertebrae also indicates that *Nhandumirim waldsangae* was not fully-grown. Irmis (2007) observed that pseudosuchians have a caudal–cranial sequence of neurocentral suture closure, but that bird-line archosaurs have a wider range of closure patterns. As such, a caudal–cranial sequence of neurocentral suture closure, although reported in some dinosaurs (Ikejiri, 2003; Irmis, 2007), cannot be assumed a priori for *Nhandumirim waldsangae*. However, the lack of neural arches in all but one of its trunk and sacral vertebrae suggests that the neurocentral sutures of these vertebrae were still open. On the other hand, the neural arches were preserved in all recovered caudal vertebrae of *Nhandumirim waldsangae*, with their neurocentral sutures closed. This suggests a caudal–cranial pattern of sutural closure in *Nhandumirim waldsangae*. According to this model, the holotype of *Nhandumirim waldsangae* would be regarded as an immature individual.

Because of its ontogenetic stage, *Nhandumirim waldsangae* might be thought to represent a juvenile of *Saturnalia tupiniquim* or *Staurikosaurus pricei*, other early saurischian dinosaurs found in the same beds, from the same or nearby sites. However, their morphological differences are noteworthy. *Nhandumirim waldsangae* differs from *Saturnalia tupiniquim* in the following traits: the presence of a ventral keel in the proximal caudal vertebrae; a short brevis fossa; no ridge connecting the brevis fossa to the iliac body and supracetabular crest; a perforated and deeper iliac acetabulum; a caudoventrally oriented ischiadic peduncle of the ilium; femur more than twice the length of the ilium; femoral head more than twice as long as wide; a short dorsolateral trochanter; no trochanteric shelf; epipodium longer than the propodium; a mediolaterally expanded distal end of the tibia; tabular caudolateral flange; a caudomedial notch on the distal margin of the tibia; a flat caudodistal margin of the

tibia; a craniomedial articular facet in the distal fibula; and a straight metatarsal IV. Compared to *Staurikosaurus pricei*, *Nhandumirim waldsangae* has the following differences: craniocaudally longer caudal trunk vertebrae; a ventral keel in the proximal caudal vertebrae; short zygapophyses in distal caudal vertebrae; a postacetabular ala longer than the iliac body; a well-developed brevis fossa; a shorter pubic peduncle; femoral head more than twice as long craniocaudally as transversely wide; short dorsolateral trochanter; mediolaterally expanded distal end of the tibia; a tabular caudolateral flange of the tibia; a caudomedial notch in the distal articulation of the tibia; a flat caudodistal margin of the tibia; and a craniomedial articular facet in the distal portion of the fibula.

We consider it unlikely that the differences above can be explained solely by ontogeny. The most recent studies on skeletal variation throughout dinosauromorph growth reveal that morphological disparity among different ontogenetic stages is limited to a more restricted range of variation than that seen between *Nhandumirim waldsangae* and either *Saturnalia tupiniquim* or *Staurikosaurus pricei*. Piechowski et al. (2014) reported morphological variation possibly related to sexual dimorphism in *Silesaurus opolensis*, where additional ossification areas, such as the trochanteric shelf (or lateral ossification), were regarded as female traits. Griffin and Nesbitt (2016a) reported that several scars on the proximal end of the femur of the silesaurid *Asilisaurus kongwe* follow a consistent developmental order. Griffin and Nesbitt (2016b) showed that the neotheropods *Coelophysis bauri* and "*Syntarsus*" *rhodesiensis* have both highly variable ontogenetic trajectories, where most of those variations (Griffin and Nesbitt, 2016b) are related to the presence of secondary ossifications and the fusion of elements in adult individuals. Compared to the ontogenetic trajectory inferred for *Asilisaurus kongwe* (Griffin and Nesbitt, 2016a), *Nhandumirim waldsangae* has features that better match

those expected for mature individuals. Also, our understanding of the anatomy of *Nhandumirim waldsangae*, *Saturnalia tupiniquim* and *Staurikosaurus pricei* suggests that these dinosaurs have neither secondary ossifications nor fusion of elements such as those described for some neotheropods (Griffin and Nesbitt, 2016b). Consequently, most of those ontogenetic variations do not match the differences between *Nhandumirim waldsangae* and either *Saturnalia tupiniquim* or *Staurikosaurus pricei*, supporting the recognition of the former as a new early dinosaur species.

Phylogenetic Analyses and Implications

Nhandumirim waldsangae was scored in two recent phylogenetic data matrixes. First, it was included in the dataset of Cabreira et al. (2016) to evaluate its relationships among early dinosauromorphs, and then it was included in the dataset of Nesbitt and Ezcurra (2015) to assess its possible theropod affinities.

Some scorings from the dataset of Cabreira et al. (2016) have been modified based on our own first-hand observations (Supplementary Data 1, Appendix 1S). Characters 256 and 257 of the modified Cabreira et al. (2016) dataset were taken from the datasets of Nesbitt and Ezcurra (2015) and Ezcurra and Brusatte (2011), respectively, because they describe features that are similarities between *Nhandumirim waldsangae* and some theropods. Character 248 from the Cabreira et al. (2016) dataset was excluded because it was considered uninformative, and a new character, number 258 of the modified Cabreira et al. (2016), was added (Supplementary Data 1, Appendix 2S). The modified Cabreira et al. (2016) data matrix is composed of 258 characters, 31 of which were ordered, and 44 taxa (Supplementary Data 1, Appendix 3S). The data matrix was analyzed in TNT 1.5 beta (Goloboff and Catalano, 2016). The heuristic search was performed under the following parameters: 10,000 replications of Wagner

Trees (with random addition sequence); TBR (tree bi-section and reconnection) for branch swapping; hold = 20 (trees saved per replicate); and collapse of zero length branches according to "rule 1" in TNT (Coddington & Scharff, 1994; Goloboff et al., 2008). The resulting MPTs were subject to a second round of TBR to ensure all MPTs are found. The TNT command-line *best* was carried out to exclude suboptimal trees.

The analysis resulted in 48 MPTs of 847 steps (Consistency Index = 0.348 and Retention Index = 0.639). The strict consensus tree (Fig. 18A) shows the same relationships outside Saurischia as those recovered by Cabreira et al. (2016). Saurischia is composed of two main clades, with Herrerasauria as the sister group of all other members of the group. *Daemonosaurus chauliodus*, *Tawa hallae* + *Chindesaurus bryansmalli* and *Eodromaeus murphi* are other saurischian dinosaurs outside Eusaurischia.*Guaibasaurus candelariensis* is recovered in two alternative positions: either outside Eusaurischia or within Sauropodomorpha. *Nhandumirim waldsangae* is found within Theropoda, as the sister taxon to a poorly resolved Neotheropoda (with a large polytomy including *Dilophosaurus wetherelli*, Petrified Forest Theropod, *Zupaysaurus rougieri*, *Liliensternus liliensterni* and coelophysoids). The relationships within Sauropodomorpha are the same as those of Cabreira et al. (2016). Bremer support values and bootstrap indices are generally low (Fig. 18A).

Based on the modified dataset of Cabreira et al. (2016), the position of *Nhandumirim waldsangae* within Theropoda is supported by three synapomorphies: a caudally extended ischiadic peduncle; a mediolaterally expanded distal end of the tibia; and a tabular caudolateral flange of the tibia. This reveals that some typical neotheropod traits, previously only known in Norian taxa, first emerged during the Carnian.

A IterPCR analyses (Pol & Escapa, 2009) shows the Petrified Forest Theropod as the main floating taxon within Neotheropoda. Its pruning results in a polytomy

including *Dilophosaurus wetherelli*, *Zupaysaurus rougieri*, and a clade where *Liliensternus liliensterni* is sister to coelophysoids.

The phylogenetic position of the problematic early dinosaur *Guaibasaurus candelariensis* (see Ezcurra, 2010; Langer et al., 2011) is different from that found by Cabreira et al. (2016). In the new analysis, its placement within Eusaurischia is supported by three synapomorphies: a short scapular blade, a more robust metacarpal I and an iliac supraacetabular crest with maximum breadth at the center of the acetabulum.

For the second analysis, some scorings were modified from the dataset of Nesbitt and Ezcurra (2015) (Supplementary Data 1, Appendix 4S), but no characters were edited or added. The data matrix was analyzed using the same search parameters described for the first analysis. This resulted in 48 MPTs each with a length of 1063 steps (Consistency Index = 0.386 and Retention Index = 0.685). Bremer support and bootstrap indexes are higher when compared to those of the first analysis (Fig. 18B). The strict consensus tree (Fig. 18B) is remarkably different from that presented by Nesbitt and Ezcurra (2015) for relationships within Saurischia, but the relationships outside of that clade match those found by those authors. The new topology shows two monophyletic groups, Sauropodomorpha and Theropoda (including *Tawa hallae*), in a large polytomy with *Nhandumirim waldsangae*, *Eodromaeus murphi*, *Eoraptor lunensis*, *Chindesaurus bryansmalli*, *Staurikosaurus pricei* and *Herrerasaurus ischigualastensis*. In this context, some characters seen both in *Nhandumirim waldsangae* and in neotheropods, including the diagonal tuberosity on the anterior surface of the distal end of the tibia, the tabular caudolateral flange and the caudomedial notch on the distal end of the tibia are interpreted as homoplastic.

The IterPCR analyses (Pol and Escapa, 2009) identified *Nhandumirim waldsangae*, *Eodromaeus murphi* and *Chindesaurus bryansmalli* as the main floating taxa. When these taxa are pruned, the new strict consensus tree recovers *Eoraptor lunensis* as a saurischian, forming a polytomy with Sauropodomorpha and Theropoda, with Herrerasauridae found as sister group of all other members of the latter group. The analysis shows three possible positions for *Nhandumirim waldsangae*: as sister taxon to Saurischia (non-Eusaurischia); as sister taxon to *Eoraptor lunensis*, in a polytomy with Sauropodomorpha and Theropoda; or as an early theropod dinosaur, sister taxon to Herrerasauridae + *Tawa hallae* + Neotheropoda. The position of *Eodromaeus murphi* is ambiguous, with possible non-herrerasaurid theropod and Herrerasauridae affinities.

Further exploratory analyses were performed under the same search parameters described above, but enforcing constraints for the monophyly between *Nhandumirim waldsangae* and *Saturnalia tupiniquim*, and *Nhandumirim waldsangae* and *Staurikosaurus pricei*. The results show that 4 extra steps are needed to recover a *Nhandumirim waldsangae* + *Saturnalia tupiniquim* clade using both the modified matrixes of Cabreira et al. (2016) and Nesbitt and Ezcurra (2015). Using, the same data matrixes, 12 and 4 extra steps are needed to recover a clade comprising *Nhandumirim waldsangae* + *Staurikosaurus pricei*.

CONCLUSIONS

The last decade has witnessed a significant increase in the record of Carnian dinosaurs, with the discoveries of *Panphagia protos*, *Chromogisaurus novasi*, *Pampadromaeus barberenais*, and *Buriolestes schultzi*. These new discoveries support new models for the rise of dinosaurs, where the group, despite not being the most

abundant faunal components, attained a noteworthy taxic diversity early in its evolutionary history (Brusatte et al., 2008a, b; Ezcurra, 2010; Benton et al., 2014).

Although incomplete, the skeletal remains of *Nhandumirim waldsangae* reveal a unique combination of potential autapomorphies, dinosauromorph and saurischian symplesiomorphies, along with features previously considered to occur exclusively within coelophysoid dinosaurs. Probably due to this incompleteness, the phylogenetic analysis recovered uncertain relations for *Nhandumirim waldsangae*, but suggest a possible closer relationship with theropods than with sauropodomorph dinosaurs. These possible theropod affinities provide clues about the emergence of some coelophysoid anatomical traits. In addition, this would represent the oldest record of Theropoda known in Brazil.

ACKNOWLEDGMENTS

JCAM is very thankful to the researchers, collection managers and curators who provided access to the collections under their care, namely: A. Turner, A. Kramarz, A. M. Ribeiro and J. Ferigolo, C. Mehling, C. Buttler, C. L. Schultz, C. Hildebrandt, D. Hutchinson, G. Cisterna, I. Werneburg, J. Powell, J. Cundiff, M. Brandalise de Andrade, O. Rauhut, R. Schoch, R. Martínez, S. Chapman, S. Cabreira, S. Jirah, T. Schossleitner, T. Sulej and M. Talanda, and Z. Erasmus. This research was supported by the following grants: FAPESP 2013/23114-1 and 2016/02473-1 to JCAM, and 2014/03825-3 to MCL; FAPEMIG APQ-01110-15 to JSB; Marie Curie Career Integration Grant (PCIG14-GA-2013-630123) to RJB. The editor M. D'Emic, F. Agnolín, H. Sues and B. Peecook are thanked for their comprehensive comments and

improvements to the paper. TNT 1.5 is a free program made available by the Willi Hennig Society, which is thanked.

LITERATURE CITED

Agnolín, F. F., and S. Rozadilla. 2017. Phylogenetic reassessment of *Pisanosaurus mertii* Casamiquela, 1967, a basal dinosauriform from the Late Triassic of Argentina. Journal of Systematic Palaeontology DOI 10.1080/14772019.2017.1352623.

Alcober, O., and R. Martínez. 2010. A new herrerasaurid (Dinosauria, Saurischia) from the Upper Triassic Ischigualasto Formation of northwestern Argentina. ZooKeys 63:1–55.

Andrade, R. C. L. P., and J. M. Sayão. 2014. Paleohistology and lifestyle inferences of a dyrosaurid (Archosauria: Crocodylomorpha) from Paraíba Basin (Northeastern Brazil). PLoS ONE 9: e102189.

Andreis, R. R., G. E. Bossi, and D. K. Montardo. 1980. O Grupo Rosário do Sul (Triássico) no Rio Grande do Sul. Congresso Brasileiro de Geologia 31:659–673.

Apaldetti, C., D. Pol, and A. Yates. 2013. The postcranial anatomy of *Coloradisaurus brevis* (Dinosauria: Sauropodomorpha) from the Late Triassic of Argentina and its phylogenetic implications. Palaeontology 56:277–301.

Baron, M. G. 2017. *Pisanosaurus mertii* and the Triassic ornithischian crisis: could phylogeny offer a solution?. Historical Biology DOI 10.1080/08912963.2017.1410705.

Baron, M. G., D. B. Norman, and P. M. Barrett. 2017. Postcranial anatomy of *Lesothosaurus diagnosticus* (Dinosauria: Ornithischia) from the Lower Jurassic of

southern Africa: implications for basal ornithischian taxonomy and systematics. Zoological Journal of the Linnean Society 179:125–168.

Benton, M. J., J. Forth, and M. C. Langer. 2014. Models for the rise of the dinosaurs. Current Biology 24:R87–R95.

Bittencourt, J. S., and A. W. A. Kellner. 2009. The anatomy and phylogenetic position of the Triassic dinosaur *Staurikosaurus pricei* Colbert, 1970. Zootaxa 2079:e56.

Bittencourt, J. S., A. B. Arcucci, C. A. Marsicano, and M. C. Langer. 2015. Osteology of the Middle Triassic archosaur *Lewisuchus admixtus* Romer (Chañares Formation, Argentina), its inclusivity, and relationships amongst early dinosauromorphs. Journal of Systematic Palaeontology 13:189–219.

Brusatte, S. L., M. J. Benton, M. Ruta, and G. T. Lloyd. 2008a. Superiority, competition, and opportunism in the evolutionary radiation of dinosaurs. Science 321:1485–1488.

Brusatte, S. L., M. J. Benton, M. Ruta, and G. T. Lloyd. 2008b. The first 50 Myr of dinosaur evolution: macroevolutionary pattern and morphological disparity. Biology Letters 4:733–736.

Brusatte, S. L., S. J. Nesbitt, R. B. Irmis, R. J. Butler, M. J. Benton, and M. A. Norell. 2010. The origin and early radiation of dinosaurs. Earth-Science Reviews 101:68–100.

Butler, R. J. 2010. The anatomy of the basal ornithischian dinosaur *Eocursor parvus* from the lower Elliot Formation (Late Triassic) of South Africa. Zoological Journal of the Linnean Society 160:648–684.

Cabreira, S. F., C. L. Schultz, J. S. Bittencourt, M. B. Soares, D. C. Fortier, L. R. Silva, and M. C. Langer. 2011. New stem-sauropodomorph (Dinosauria, Saurischia) from the Triassic of Brazil. Naturwissenschaften 98:1035–1040.

Cabreira, S. F., A. W. A. Kellner, S. Dias-da-Silva, L. R. da Silva, M. Bronzati, J. C. A. Marsola, R. T. Müller, J. S. Bittencourt, B. J. Batista, T. Raugust, R. Carrilho, A. Brodt, and M. C. Langer. 2016. A Unique Late Triassic Dinosauromorph Assemblage Reveals Dinosaur Ancestral Anatomy and Diet. Current Biology 26:3090–3095.

Casamiquela, R. M. 1967. Un nuevo dinosaurio ornitisquio Triásico (*Pisanosaurus mertii*; Ornithopoda) de la Formacion Ischigualasto, Argentina. Ameghiniana 5:47–64.

Cherry, C. 2002. Bone histology of the primitive dinosaur, *Thecodontosaurus antiquus*. M.Sc. thesis, University of Bristol, Bristol, 68 pp.

Chinsamy, A. 1993. Bone histology and growth trajectory of the prosauropod dinosaur *Massospondylus carinatus* Owen. Modern Geology, 18:319–219.

Coddington, J., and N. Scharff. 1994. Problems with zero-length branches. Cladistics 10: 415–423.

Colbert, E. H. 1970. A saurischian dinosaur from the Triassic of Brazil. American Museum Novitates 2405:1–60.

Curry, K. A. 1999. Ontogenetic histology of *Apatosaurus* (Dinosauria: Sauropoda): new insights on growth rates and longevity. Journal of Vertebrate Paleontology 19:654–665.

Da Rosa, Á. A. S. 2004. Sítios fossilíferos de Santa Maria, RS. Ciência & Natura 26:75–90.

Da Rosa, Á. A. S. 2005. Paleoalterações em depósitos sedimentares de planícies aluviais do Triássico Médio a Superior do sul do Brasil: caracterização, análise estratigráfica e preservação fossilífera. PhD dissertation, Universidade do Vale dos Sinos, São Leopoldo, 211 pp.

Da Rosa, Á. A. S. 2015. Geological context of the dinosauriform-bearing outcrops from the Triassic of Southern Brazil. Journal of South American Earth Sciences 61:108–119.

de Ricqlès, A., K. Padian, F. Knoll, and J. R. Horner. 2008. On the origin of high growth rates in archosaurs and their ancient relatives: Complementary histological studies on Triassic archosauriforms and the problem of a "phylogenetic signal" in bone histology. Annales de Paleontologie 94:57–76.

Eltink, E., Á. A. S. Da Rosa, and S. Dias-da-Silva. 2016. A capitosauroid from the Lower Triassic of South America (Sanga do Cabral Supersequence: Paraná Basin), its phylogenetic relationships and biostratigraphic implications. Historical Biology 29:863–874.

Erickson, G. 2005. Assessing dinosaur growth patterns: a microscopic revolution. Trends in Ecology & Evolution 20:677–684.

Erickson, G. M., and T. A. Tumanova. 2000. Growth curve of *Psittacosaurus mongoliensis* Osborn (Ceratopsia: Psittacosauridae) inferred from long bone histology. Zoological Journal of the Linnean Society 130:551–566

Ezcurra, M. D. 2010. A new early dinosaur (Saurischia: Sauropodomorpha) from the Late Triassic of Argentina: a reassessment of dinosaur origin and phylogeny. Journal of Systematic Palaeontology 8:371–425.

Ezcurra, M. D. 2012. Comments on the taxonomic diversity and paleobiogeography of the earliest known dinosaur assemblages (late Carnian-earliest Norian). Historia Natural, tercera serie 2:49–71.

Ezcurra, M. D., and F. E. Novas. 2007. Phylogenetic relationships of the Triassic theropod *Zupaysaurus rougieri* from NW Argentina. Historical Biology 19:35–72.

Ezcurra, M. D., and S. L. Brusatte. 2011. Taxonomic and phylogenetic reassessment of the early neotheropod dinosaur *Camposaurus arizonensis* from the Late Triassic of North America. Palaeontology 54:763–772.

Ezcurra, M. D., and C. Apaldetti. 2012. A robust sauropodomorph specimen from the Upper Triassic of Argentina and insights on the diversity of the Los Colorados Formation. Proceedings of the Geologists' Association 123:155–164.

Fostowicz-Frelik, Ł., and T. Sulej. 2010: Bone histology of *Silesaurus opolensis* Dzik, 2003 from the Late Triassic of Poland. Lethaia 43:137–148.

Francillon-Vieillot, H. J., W. Arntzen, and J. Geraudie. 1990. Age, growth and longevity of sympatric *Triturus cristatus*, *Triturus marmoratus* and their hybrids (Amphibia, Urodela): A skeletochronological comparison. Journal of Herpetology 24:13–22.

Fraser, N. C., K. Padian, G. M. Walkden, and A. L. M. Davis. 2002. Basal dinosauriform remains from Britain and the diagnosis of the Dinosauria. Palaeontology 45:79–95.

Gatesy, S. M. 1990. Caudofemoral musculature and the evolution of theropod locomotion. Paleobiology 16:170–186.

Gauthier, J.A. 1986. Saurischian monophyly and the origin of birds. Memoirs of the California Academy of Science 8:1–55.

Goloboff, P. A., and S. A. Catalano. 2016. TNT version 1.5, including a full implementation of phylogenetic morphometrics. Cladistics 32:221–238.

Goloboff, P. A., J. S. Farris, and K. C. Nixon. 2008. TNT, a free program for phylogenetic analysis. Cladistics 24:774–786.

Gordon Jr., M. 1947. Classificação das formações gondwânicas do Paraná, Santa Catarina e Rio Grande do Sul. Notas Preliminares e Estudos, DNPM/DGM, Rio de Janeiro 38:1–20.

Griffin, C. T., and S. J. Nesbitt. 2016a. The femoral ontogeny and long bone histology of the Middle Triassic (? late Anisian) dinosauriform *Asilisaurus kongwe* and implications for the growth of early dinosaurs. Journal of Vertebrate Paleontology 36:e1111224.

Griffin, C. T., and S. J. Nesbitt. 2016b. Anomalously high variation in postnatal development is ancestral for dinosaurs but lost in birds. Proceedings of the National Academy of Sciences 113 and 14757–14762.

Horn, B. L. D., T. M. Melo, C. L. Schultz, R. P. Philipp, H. P. Kloss, and K. Goldberg. 2014. A new third-order sequence stratigraphic framework applied to the Triassic of the Paraná Basin, Rio Grande do Sul, Brazil, based on structural, stratigraphic and paleontological data. Journal of South American Earth Sciences 55:123–132.

Horner, J. R., A. de Ricqlès, and K. Padian. 2000. Long bone histology of the hadrosaurid dinosaur *Maiasaura peeblesorum*: growth dynamics and physiology based on an ontogenetic series of skeletal elements. Journal of Vertebrate Paleontology 20:115–129.

Horner, J. R., K. Padian, and A. de Ricqlès. 2001. Comparative osteohistology of some embryonic and neonatal archosaurs: implications for variable life histories among dinosaurs. Paleobiology 27:39–58.

Huene, F. v. 1928. Ein Cynodotier aus des Trias Brasilensis. Centralblatt für Mineralogie, Geologie und Paläontologie 1928B:251-270.

Huene, F. v. 1942. Die fossilen Reptilien des Südamerikanischen Gondwanalandes. Ergebnisse der Sauriergrabungen in Südbrasilien, 1928/1929. Munich: C. H. Beck'sche Verlagsbuchhandlung 1942.

Hutchinson, J. R. 2001a. The evolution of pelvic osteology and soft tissues on the line to extant birds (Neornithes). Zoological Journal of the Linnean Society 131:123–168.

Hutchinson, J.R. 2001b. The evolution of femoral osteology and soft tissues on the line to extant birds (Neornithes). Zoological Journal of Linnean Society 131:169–197.

Ikejiri, T. 2003. Sequence of closure of neurocentral sutures in *Camarasaurus* (Sauropoda) and implications for phylogeny in Reptilia. Journal of Vertebrate Paleontology 23(3 Supplement):65A.

Irmis, R. B. 2007. Axial skeleton ontogeny in the Parasuchia (Archosauria: Pseudosuchia) and its implications for ontogenetic determination in archosaurs. Journal of Vertebrate Paleontology 27:350–361.

Klein, N., and P. M. Sander. 2007. Bone histology and growth of the prosauropod *Plateosaurus engelhardti* Meyer, 1837 from the Norian bonebeds of Trossingen (Germany) and Frick (Switzerland). Special Papers in Palaeontology 77:169–206.

Klein, N., P. M. Sander, K. Stein, J. Le Loeuff, J. L. Carballido, and E. Buffetaut. 2012. Modified laminar bone in *Ampelosaurus atacis* and other titanosaurs (Sauropoda): implications for life history and physiology. PLoS ONE 7:e36907.

Lamm, E-T. 2013. Bone Histology of Fossil Tetrapods; pp. 55–160 in K. Padian and T-T. Lamm (eds.), Preparation and Sectioning of Specimens. University of California Press, Berkeley, California.

Langer, M. C. 2003. The pelvic and hind limb anatomy of the stem-sauropodomorph *Saturnalia tupiniquim* (Late Triassic, Brazil). PaleoBios 23:1–40.

Langer, M. C. 2004. Basal Saurischia. Pp. 25–46 in D. B. Weishampel, P. Dodson & H. Osmolska (eds) The Dinosauria, 2nd edition. University of California Press, Berkeley.

Langer, M. C. 2005a. Studies on continental Late Triassic tetrapod biochronology. I. The type locality of *Saturnalia tupiniquim* and the faunal succession in south Brazil. Journal of South American Earth Sciences 19:205–218.

Langer, M. C. 2005b. Studies on continental Late Triassic tetrapod biochronology. II. The Ischigualastian and a Carnian global correlation. Journal of South American Earth Sciences 19:219–239.

Langer, M. C., and M. J. Benton. 2006. Early dinosaurs: a phylogenetic study. Journal of Systematic Palaeontology 4:309–358.

Langer, M. C., and J. Ferigolo. 2013. The Late Triassic dinosauromorph *Sacisaurus agudoensis* (Caturrita Formation; Rio Grande do Sul, Brazil): anatomy and affinities. Geological Society, London, Special Publications 379:353–392.

Langer, M. C., F. Abdala, M. Richter, and M. J. Benton. 1999. A sauropodomorph dinosaur from the Upper Triassic (Carman) of southern Brazil. Comptes Rendus de l'Académie des Sciences-Series IIA-Earth and Planetary Science 329:511–517.

Langer, M. C., A. M. Ribeiro, C. L. Schultz, and J. Ferigolo. 2007. The continental tetrapod-bearing Triassic of South Brazil. New Mexico Museum of Natural History and Science Bulletin 41:201–218.

Langer, M. C., M. D. Ezcurra, J. S. Bittencourt, and F. E. Novas. 2010a. The origin and early evolution of dinosaurs. Biological Reviews 85:55–110.

Langer, M. C., J. S. Bittencourt, and C. L. Schultz. 2010b. A reassessment of the basal dinosaur *Guaibasaurus candelariensis*, from the Late Triassic Caturrita Formation

of south Brazil. Earth and Environmental Science Transactions of the Royal Society of Edinburgh 101:301–332.

Langer, M.C., S. J. Nesbitt, J. S. Bittencourt, and R. B. Irmis. 2013. Non-dinosaurian Dinosauromorpha. Geological Society, London, Special Publications 379:157–186.

Langer, M. C., A. D. Rincón, J. Ramezani, A. Solórzano, and O. W. Rauhut. 2014. New dinosaur (Theropoda, stem-Averostra) from the earliest Jurassic of the La Quinta Formation, Venezuelan Andes. Royal Society open science 1:140184.

Langer, M. C., J. Ramezani, and Á. A. S. Da Rosa. 2018. U-Pb age constraints on dinosaur rise from south Brazil. Gondwana Research DOI 10.1016/j.gr.2018.01.005.

Marsh, O. C. 1881. Principal characters of American Jurassic dinosaurs V. American Journal of Science 16:411–416.

Martill, D. M., S. U. Vidovic, C. Howells, and J. R. Nudds. 2016. The oldest Jurassic dinosaur: a basal neotheropod from the Hettangian of Great Britain. PloS one 11:e0145713.

Martinelli, A. G., E. Eltink, Á. A. S. Da Rosa, and M. C. Langer. 2017. A new cynodont from the Santa Maria formation, south Brazil, improves Late Triassic probainognathian diversity. Papers in Palaeontology 3:401–423.

Martínez, R. N., and O. A. Alcober. 2009. A basal sauropodomorph (Dinosauria: Saurischia) from the Ischigualasto Formation (Triassic, Carnian) and the early evolution of Sauropodomorpha. PLoS One 4:e4397.

Martínez, R. N., P. C. Sereno, O. A. Alcober, C. E. Colombi, P. R. Renne, I. P. Montañez, and B. S. Currie. 2011. A basal dinosaur from the dawn of the dinosaur era in southwestern Pangaea. Science 331:206–210.

Martínez, R. N., C. Apaldetti, O. A. Alcober, C. E. Colombi, P. E. Sereno, E. Fernandez, P. S. Malnis, G. A. Correa, and D. Abelín, D. 2012. Vertebrate succession in the Ischigualasto Formation. Journal of Vertebrate Paleontology 32:10–30.

Martínez, R. N., C. Apaldetti, G. A. Correa, and D. Abelín, D. 2016. A Norian Lagerpetid Dinosauromorph from the Quebrada Del Barro Formation, Northwestern Argentina. Ameghiniana 53:1–13.

Nesbitt, S. J., N. D. Smith, R. B. Irmis, A. H. Turner, A. Downs, and M. A. Norell. 2009. A complete skeleton of a Late Triassic saurischian and the early evolution of dinosaurs. Science 326:1530–1533.

Nesbitt, S. J. 2011. The early evolution of archosaurs: relationships and the origin of major clades. Bulletin of the American Museum of Natural History, 352:1–292.

Nesbitt, S. J., and M. D. Ezcurra. 2015. The early fossil record of dinosaurs in North America: A new neotheropod from the base of the Upper Triassic Dockum Group of Texas. Acta Palaeontologica Polonica 60:513–526.

Norman, D. B., L. M. Witmer, and D. B. Weishampel. 2004. Basal ornithischia. Pp. 325–334 in D. B. Weishampel, P. Dodson & H. Osmolska (eds) The Dinosauria, 2nd edition. University of California Press.

Novas, F. E. 1992. Phylogenetic relationships of the basal dinosaurs, the Herrerasauridae. Palaeontology 35:51-62.

Novas, F. E. 1994. New information on the systematics and postcranial skeleton of *Herrerasaurus ischigualastensis* (Theropoda: Herrerasauridae) from the Ischigualasto Formation (Upper Triassic) of Argentina. Journal of Vertebrate Paleontology 13:400–423.

Novas, F. E. 1996. Dinosaur monophyly. Journal of vertebrate Paleontology 16:723–741.

Owen, R. 1842. Report on British fossil reptiles, part II. Report for the British Association for the Advancement of Science, Plymouth, 1841:60–294.

Padian, K. 1988. On the type material of *Coelophysis* Cope (Saurischia: Theropoda) and a new specimen from the Petrified Forest of Arizona (Late Triassic: Chinle Formation); pp. 45-60 in K. Padian (ed.), The beginning of the age of dinosaurs: faunal change across the Triassic-Jurassic boundary. Cambridge University Press, New York, New York.

Padian, K. and C. L. May. 1993. The earliest dinosaurs; pp. 379–382 in S. G. Lucas and M. Morales M. (eds.), The Nonmarine Triassic. Bulletin of the New Mexico Museum of Natural History and Science, Albuquerque, New Mexico.

Peecook, B. R., C. A. Sidor, S. J. Nesbitt, R. M. Smith, J. S. Steyer, and K. D. Angielczyk. 2013. A new silesaurid from the upper Ntawere Formation of Zambia (Middle Triassic) demonstrates the rapid diversification of Silesauridae (Avemetatarsalia, Dinosauriformes). Journal of Vertebrate Paleontology 33:1127–1137.

Peecook, B. R., J. S. Steyer, N. J. Tabor, and M. H. Smith. 2017. Updated geology and vertebrate paleontology of the Triassic Ntawere Formation of northeastern Zambia, with special emphasis on the archosauromorphs, Journal of Vertebrate Paleontology 37: 8–38.

Piechowski, R., M. Tałanda, and J. Dzik. 2014. Skeletal variation and ontogeny of the Late Triassic dinosauriform *Silesaurus opolensis*. Journal of Vertebrate Paleontology 34:1383–1393.

Pol, D., and H Escapa. 2009. Unstable taxa in cladistic analysis: identification and the assessment of relevant characters. Cladistics 25:515–527.

Pol, D., A. Garrido, and I. A. Cerda. 2011. A new sauropodomorph dinosaur from the Early Jurassic of Patagonia and the origin and evolution of the sauropod type sacrum. PLoS ONE 6:e14572. doi:10.1371/journal.pone.0014572.

Pretto, F. A., C. L. Schultz, and M. C. Langer. 2015. New dinosaur remains from the Late Triassic of southern Brazil (Candelária Sequence, *Hyperodapedon* Assemblage Zone). Alcheringa 39:264–273.

Rauhut, O. W M. 2003. The interrelationships and evolution of basal theropod dinosaurs. Special Papers in Palaeontology, 69:1–215.

Reig, O. A. 1963. La presencia de dinosaurios saurisquios en los "Estratos de Ischigualasto" (Mesotriaisico superior) de las provincias de San Juan y La Rioja (República Argentina). Ameghiniana 3:3–20.

Sander, P.M. 1999. Life history of the Tendaguru sauropods as inferred from long bone histology. Mitteilungen aus dem Museum für Naturkunde der Humboldt-Universität zu Berlin, Geowissenschaftliche Reihe 2:103–112.

Sander, P. M. 2000. Long bone histology of the Tendaguru sauropods: implications for growth and biology. Paleobiology 26:466–488.

Sander, P. M., and C. Tückmantel. 2003. Bone lamina thickness, bone apposition rates, and age estimates in sauropod humeri and femora. Paläontologische Zeitschrift 76:161–172.

Sander, P. M., and N. Klein. 2005. Developmental plasticity in the life history of a prosauropod dinosaur. Science 16:1800–1802.

Sander, P. M., N. Klein, E. Buffetaut, G. Cuny, V. Suteethorn, and J. L. Loeuff. 2004. Adaptive radiation in sauropod dinosaurs: bone histology indicates rapid

evolution of giant body size through acceleration. Organisms Diversity and Evolution 4:165–173.

Sander, P. M., N. Klein, K. Stein, and O. Wings. 2011. Sauropod bone histology and implications for sauropod biology; pp. 276–302 in N. Klein, K. Remes, C. T. Gee, and P. M. Sander (eds), Biology of the sauropod dinosaurs: understanding the life of giants. Indiana University Press, Bloomington, Indiana.

Seeley, H.G. 1887. On the classification of the fossil animals commonly named Dinosauria. Proceedings of the Royal Society of London 43:165–171.

Sereno, P. C., and A. B. Arcucci. 1993. Dinosaurian percursors from the Middle Triassic of Argentina: *Lagerpeton chanarensis*. Journal of Vertebrate Paleontology 13:385–399.

Sereno, P. C., and A. B. Arcucci. 1994. Dinosaurian precursors from the Middle Triassic of Argentina: *Marasuchus lilloensis*, gen. nov. Journal of Vertebrate Paleontology 14:53–73.

Sereno, P. C., C. A. Forster, R. R. Rogers, and A. M. Monetta. 1993. Primitive dinosaur skeleton from Argentina and the early evolution of Dinosauria. Nature 361:64–66.

Sereno, P. C., R. N. Martínez, and O. A. Alcober. 2012. Osteology of *Eoraptor lunensis* (Dinosauria, Sauropodomorpha). Journal of Vertebrate Paleontology 32:83–179.

Stein, K. 2010. Long bone histology of basalmost and derived Sauropodomorpha: the convergence of fibrolamellar bone and the evolution of giantism and nanism. PhD dissertation, University of Bonn, Bonn, 213 pp.

Stein, K., and E. Prondvai. 2014. Rethinking the nature of fibrolamellar bone: an integrative biological revision of sauropod plexiform bone formation. Biological Reviews 89:24–47.

Sues, H. D., S. J. Nesbitt, D. S. Berman, and A. C. Henrici. 2011. A late-surviving basal theropod dinosaur from the latest Triassic of North America. Proceedings of the Royal Society B 278:3459–3464.

Tykoski, R. S. 2005. Anatomy, ontogeny, and phylogeny of coelophysoid theropods. PhD dissertation, The University of Texas at Austin, Austin, 553 pp.

Welles, S. P. 1984. *Dilophosaurus wetherilli* (Dinosauria, Theropoda). Osteology and comparisons. Palaeontographica 185:85–180.

Wilson, J. A. 1999. A nomenclature for vertebral laminae in sauropods and other saurischian dinosaurs. Journal of vertebrate Paleontology 19:639–653.

Wilson, J. A. 2012. New vertebral laminae and patterns of serial variation in vertebral laminae of sauropod dinosaurs. Contributions from the Museum of Paleontology, University of Michigan 32:91–110.

Wilson, J. A., D. D. Michael, T. Ikejiri, E. M. Moacdieh, and J. A. Whitlock. 2011. A nomenclature for vertebral fossae in sauropods and other saurischian dinosaurs. PLoS One 6:e17114.

Yates, A. M. 2007. The first complete skull of the Triassic dinosaur *Melanorosaurus* Haughton (Sauropodomorpha: Anchisauria). Special Papers in Palaeontology, 77:9–55.

Zerfass, H., E. L. Lavina, C. L. Schultz, A. J. V. Garcia, U. F. Faccini, and F. Chemale. 2003. Sequence stratigraphy of continental Triassic strata of Southernmost Brazil: a contribution to Southwestern Gondwana palaeogeography and palaeoclimate. Sedimentary Geology 161:85–105.

October 20, 2017; accepted Month DD, YYYY

FIGURES

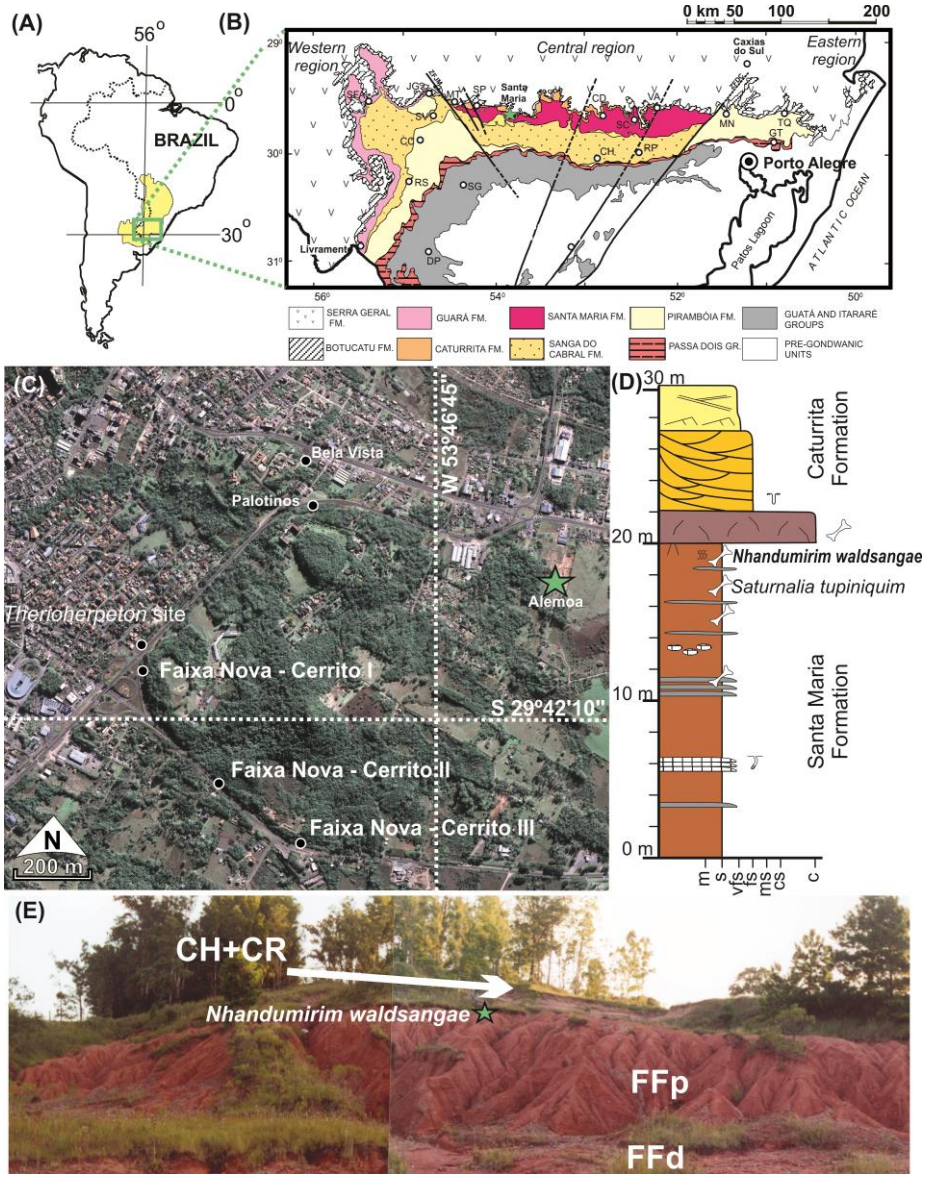

FIGURE 1. Geographic and geologic provenance of *Nhandumirim waldsangae* gen. et sp. nov. **A**, map of the Paraná Basin in South America; **B**, simplified geological map of the central portion of Rio Grande do Sul State (modified from Eltink et al., 2016), indicating Santa Maria (green star); **C**, location of selected outcrops in the eastern outskirts of Santa Maria (modified from Da Rosa, 2014), indicating the Waldsanga/Cerro da Alemoa site (green star); **D**, sedimentary log from the Waldsanga/Cerro da Alemoa outcrop, indicating the provenance of the studied specimen and other fossiliferous beds (modified from Da Rosa, 2005); **E**, photograph of the outcrop, showing the channel and crevasse deposits (CH+CR) of the Caturrita

Formation, and the distal (FFd) and proximal floodplain deposits (FFp) of the Santa Maria Formation, indicating the level where *Nhandumirim waldsangae* gen. et sp. nov. was found. [planned for page width]

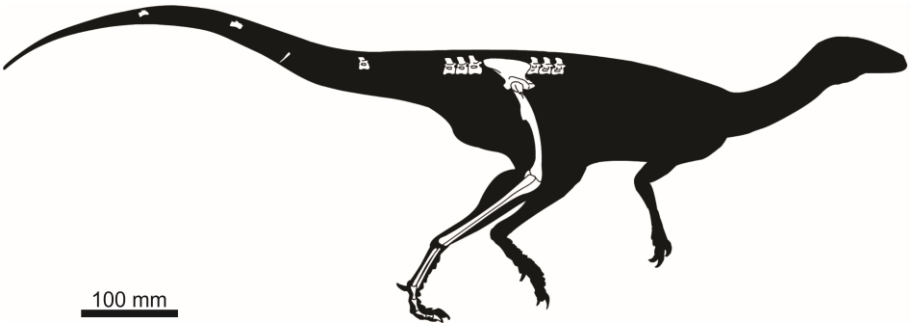

FIGURE 2. Silhouette depicting the preserved bones of *Nhandumirim waldsangae* gen. et sp. nov. (LPRP/USP 0651). [planned for page width]

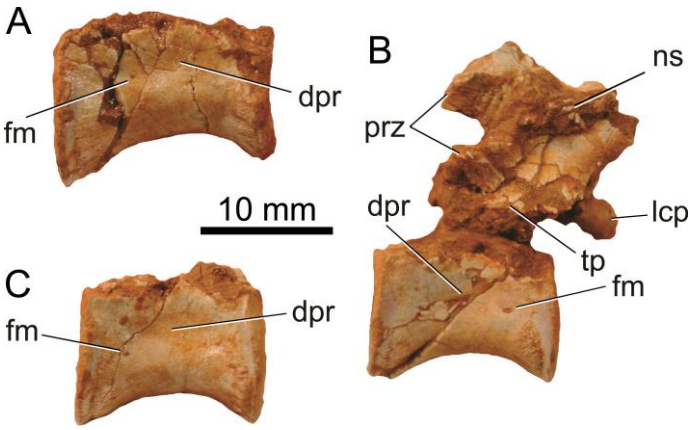

FIGURE 3. *Nhandumirim waldsangae* gen. et sp. nov. (LPRP/USP 0651). Trunk vertebrae "1"(**A**), "2" (**B**) and "3" (**C**) in right lateral (**A**) and left lateral (**B**–**C**) views. **Abbreviations**: **dpr**, depression; **fm**, foramen; **lcp**, left caudal pedicel; **ns**, neural spine; **prz**, prezygapophysis; **tp**, transverse process. [planned for column width]

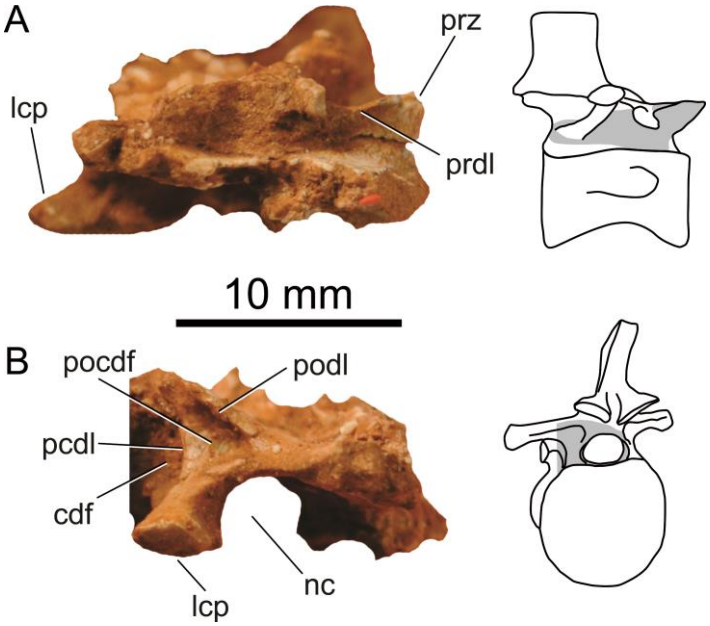

FIGURE 4. *Nhandumirim waldsangae* gen. et sp. nov. (LPRP/USP 0651). Partial neural arch of trunk vertebra "2" in (**A**) right lateral and (**B**) left caudolateral views. **Abbreviations**: **cdf**, centrodiapophyseal fossa; **lcp**, left caudal pedicel; **nc**, neural canal; **pcdl**, posterior centrodiapophyseal lamina; **pocdf**, postzygapophyseal centrodiapophyseal fossa; **podl**, postzygodiapophyseal lamina; **prdl**, prezygodiapophyseal lamina; **prz**, prezygapophysis. [planned for column width]

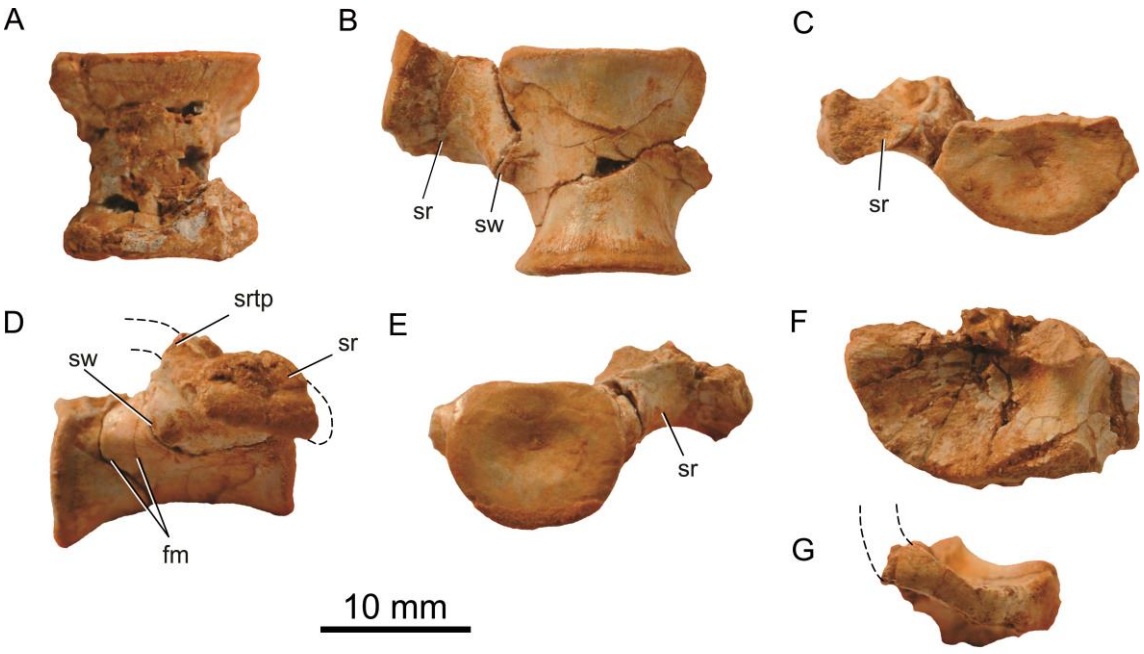

FIGURE 5. *Nhandumirim waldsangae* gen. et sp. nov. (LPRP/USP 0651). Sacral vertebrae. **A**, isolated centrum in ventral view. Second primordial sacral vertebral centrum in (**B**) ventral, (**C**) cranial, (**D**) right lateral and (**E**) caudal views. Left rib of first primordial sacral in (**F**) dorsal and (**G**) left lateral views. Dashed lines denote inferred limits of missing portions. **Abbreviations**: **fm**, foramen; **sr**, sacral rib; **srtp**, sacral rib and transverse process; **sw**, swelling. [planned for page width]

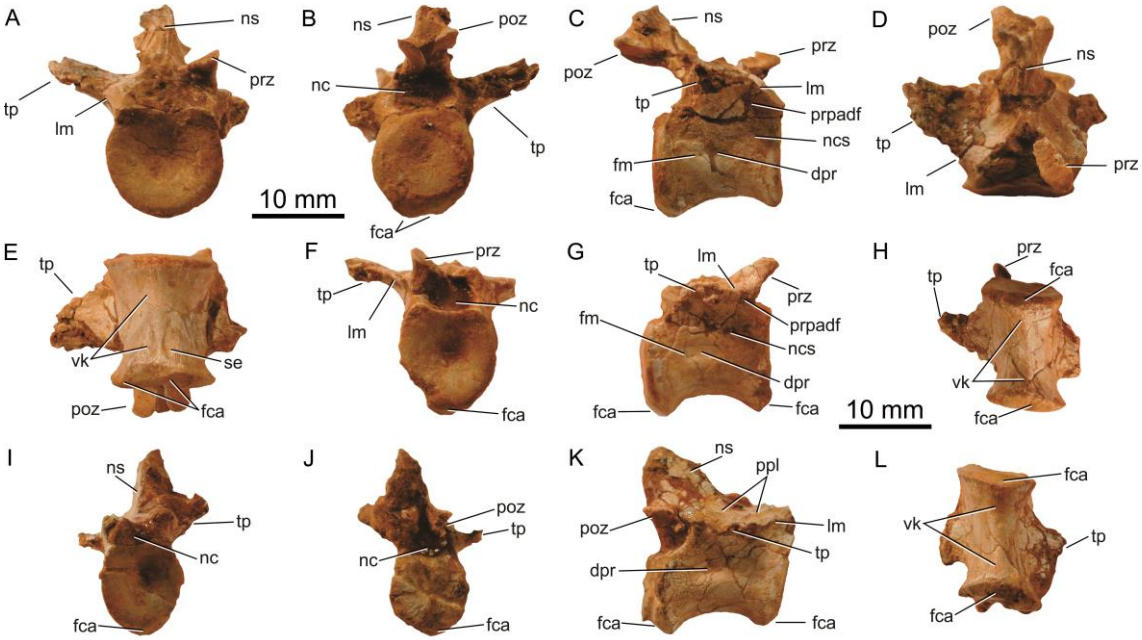

FIGURE 6. *Nhandumirim waldsangae* gen. et sp. nov. (LPRP/USP 0651). Caudal vertebrae "1" (**A**-**D**), "2" (**E**-**H**) and "3" (**I**-**L**) in (**A**, **F** and **I**) cranial, (**B** and **J**) caudal, (**C**, **G** and **K**) right lateral, (**D**) dorsal and (**E**, **H** and **L**) ventral views. **Abbreviations**: **dpr**, depression; **fca**, facet for chevron articulation; **fm**, foramen; **lm**, lamina; **nc**, neural canal; **ncs**, neurocentral suture; **ns**, neural spine; **poz**, postzygapophysis; **ppl**, prezygo-postzygopophyseal lamina; **prz**, prezygapophysis; **prpadf**, prezygapophyseal parapodiapophyseal fossa; **se**, shallow excavation; **tp**, transverse process; **vk**, ventral keel. [planned for page width]

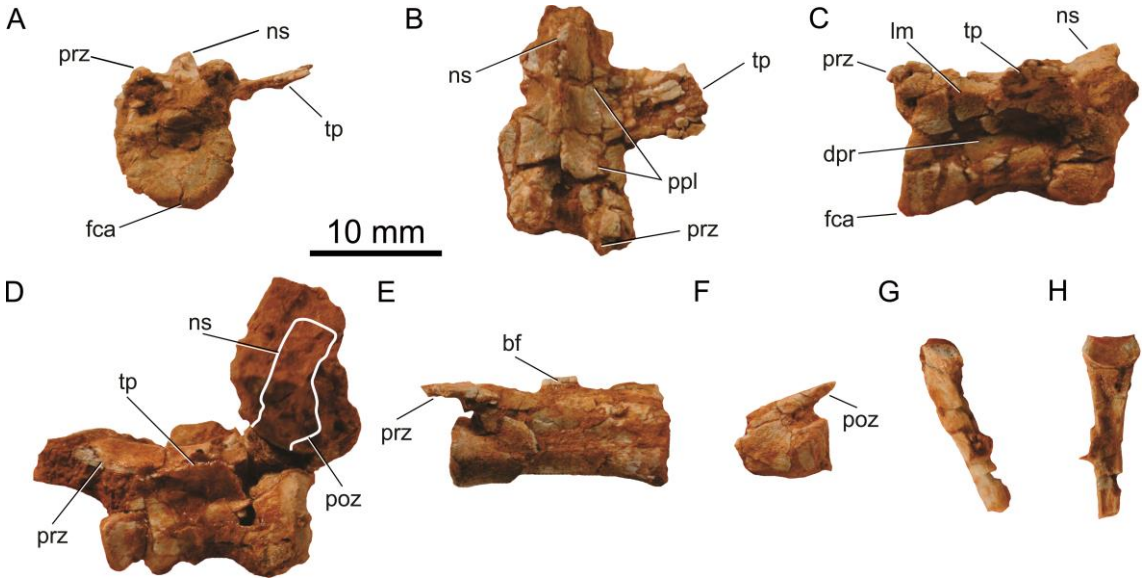

FIGURE 7. *Nhandumirim waldsangae* gen. et sp. nov. (LPRP/USP 0651) Caudal vertebrae "4" (**A**-**C**), "5" (**D**), "6" (**E**), "7" (**F**) and chevron (**G**-**H**) in (**A**) cranial, (**B**) dorsal, (**C**-**G**) left lateral and (**H**) caudal views. **Abbreviations**: **dpr**, depression; **fca**, facet for chevron articulation; **lm**, lamina; **ns**, neural spine; **poz**, postzygapophysis; **ppl**, prezygo-postzygopophyseal lamina; **prz**, prezygapophysis. [planned for page width]

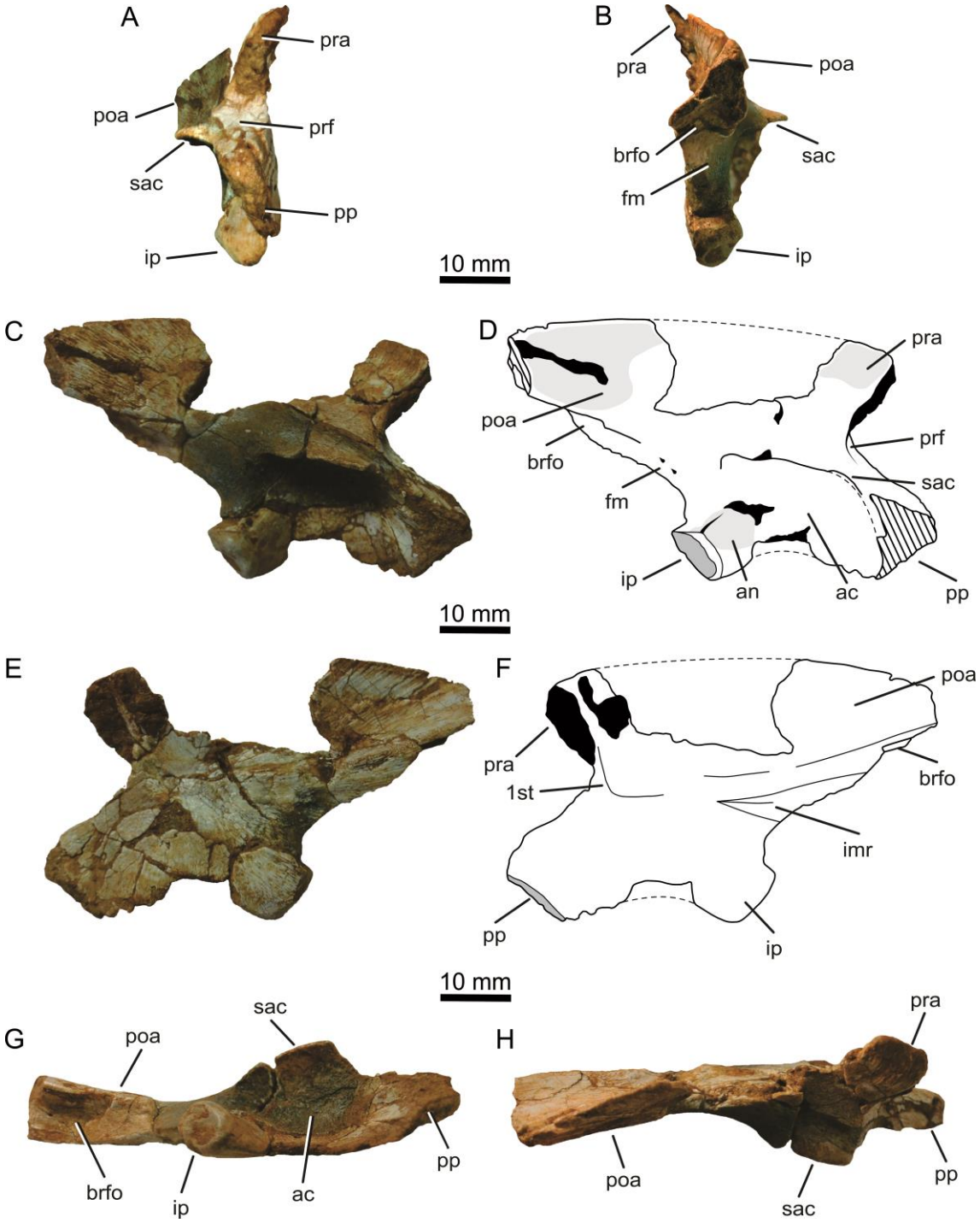

FIGURE 8. *Nhandumirim waldsangae* gen. et sp. nov. (LPRP/USP 0651). Right ilium in (**A**) cranial, (**B**) caudal, (**C** and **D**) lateral, (**E** and **F**) medial, (**G**) ventral and (**H**) dorsal views. **D** and **F** are outline drawings of **C** and **E**, respectively. Parts in black represent portions still covered by sediment; light gray represents scarred areas; dark gray represents articular facets of the peduncles; dashed lines represent the possible limits of missing parts; cross-hatched areas show broken parts. **Abbreviations**: **1st**,

attachment scars for the first primordial sacral rib; **ac**, iliac acetabulum; **an**, acetabular antitrochanter; **brfo**, brevis fossa; **fm**, foramina; **imr**, iliac medial ridges; **ip**, ischiadic peduncle; **sac**, supracetabular crest; **poa**, postacetabular ala; **pp**, pubic peduncle; **pra**, preacetabular ala; **prf**; preacetabular fossa. [planned for page width]

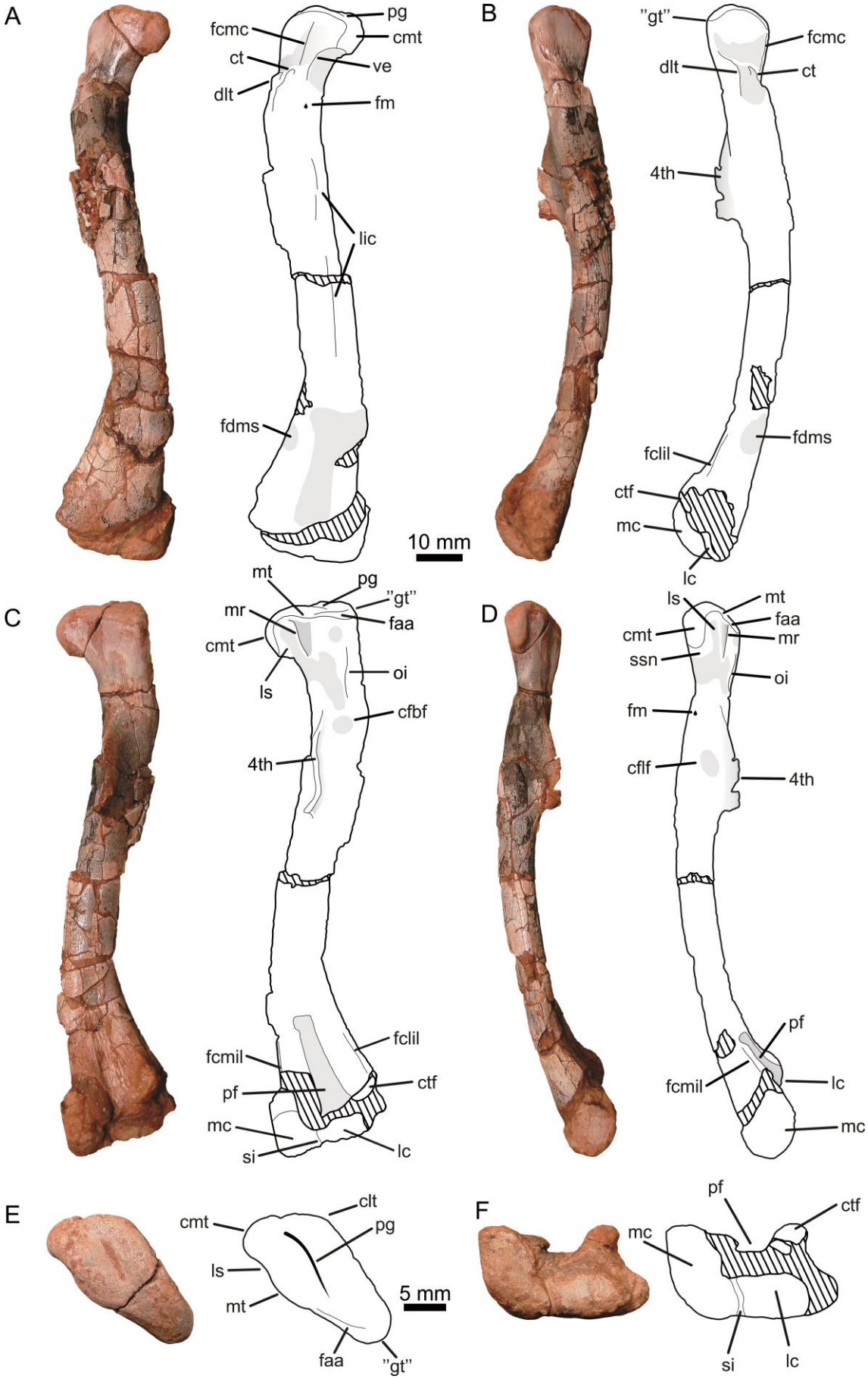
A
fcmc
pg
cmt
ct
ve
dlt
fm
lic
fdms
10 mm
B
"gt"
fcmc
dlt
ct
4th
fdms
fclil
ctf
mc
lc
C
mt
pg
"gt"
mr
faa
cmt
oi
ls
cfbf
4th
fclil
fcmil
ctf
pf
mc
si
lc
D
ls
mt
faa
cmt
mr
ssn
oi
fm
cflf
4th
pf
fcmil
lc
mc
E
clt
cmt
pg
ls
5 mm
mt
faa
"gt"
F
pf
ctf
mc
si
lc

FIGURE 9. *Nhandumirim waldsangae* gen. et sp. nov. (LPRP/USP 0651). Right femur in (**A**) cranial, (**B**) lateral, (**C**) caudal, (**D**) medial, (**E**) proximal, and (**F**) distal views. Light gray indicate scarred areas, cross-hatched areas represent broken parts. **Abbreviations**: **4th**, fourth trochanter; **clt**, craniolateral tuber; **cmt**, craniomedial tuber; **cfbf**, fossa for caudofemoralis brevis; **cflf**, fossa for caudofemoralis longus; **ct**, cranial trochanter; **ctf**, crista tibiofibularis; **dlt**, dorsolateral trochanter; **faa**, facies articularis antitrochanterica; **fclil**, femoral caudolateral intermuscular line; **fcmil**, femoral caudomedial intermuscular line; **fcmc**, femoral craniomedial crest; **fdms**, muscle scar on laterocranial distal femur; **fm**, foramen; "**gt**", great trochanter; **lc**, lateral condyle; **lic**, linea intermuscularis cranialis; **ls**, ligament sulcus; **mc**, medial condyle; **mt**, medial tuber ; **mr**, medial ridge; **oi**, obturatorius insertion; **pf**, popliteal fossa; **pg**, proximal groove; **si**, sulcus intercondylaris; **ssn**, saddle-shaped notch; **ve**, ventral emargination. [planned for page width]

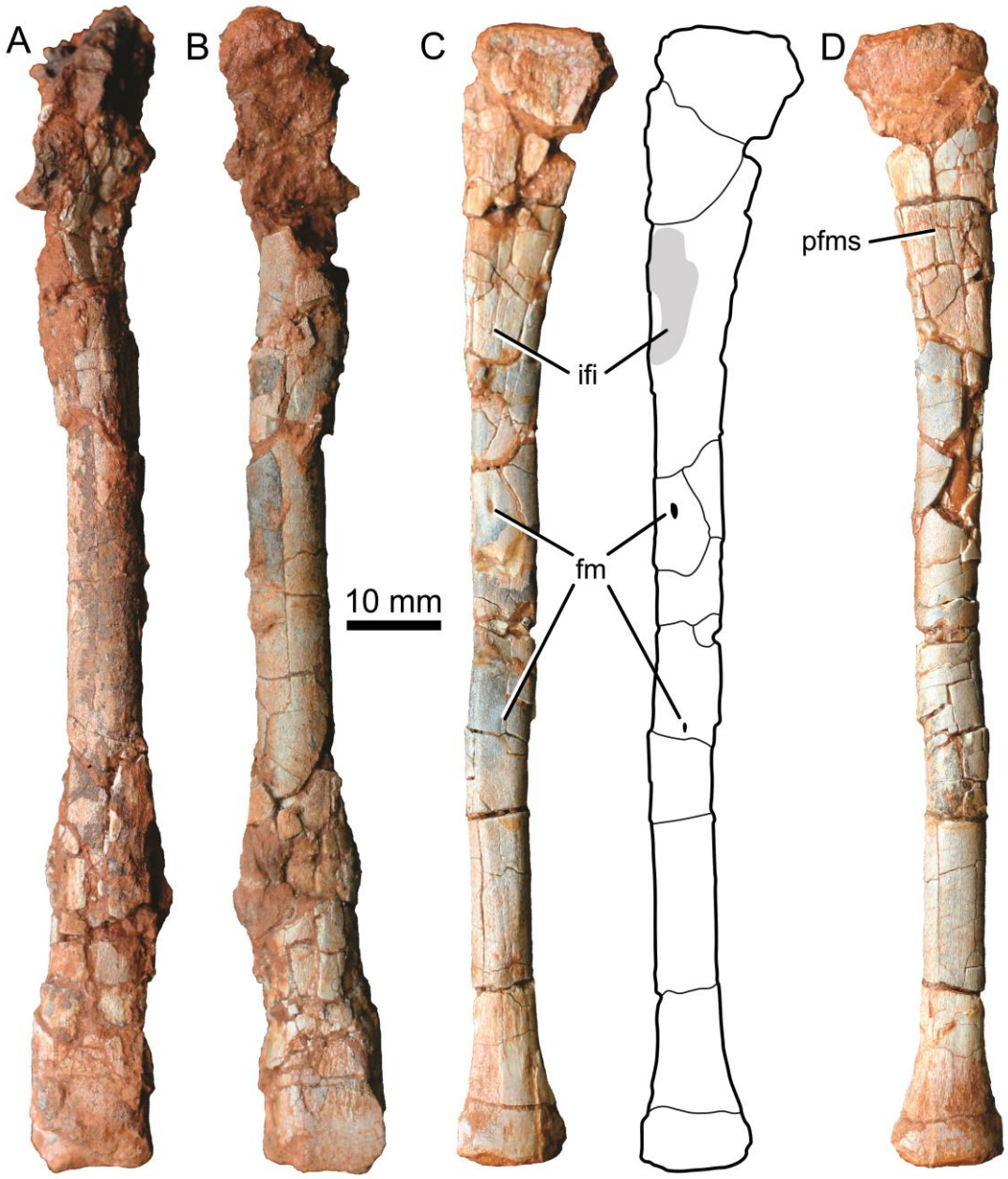

FIGURE 10. *Nhandumirim waldsangae* gen. et sp. nov. (LPRP/USP 0651). Right tibia (**A** and **B**) and fibula (**C** and **D**) in (**A** and **C**) cranial and (**B** and **D**) caudal views. **Abbreviations**: **ifi**, iliofibularis insertion; **fm**, foramina; **pfms**, muscle scars on proximal fibula. [planned for column width]

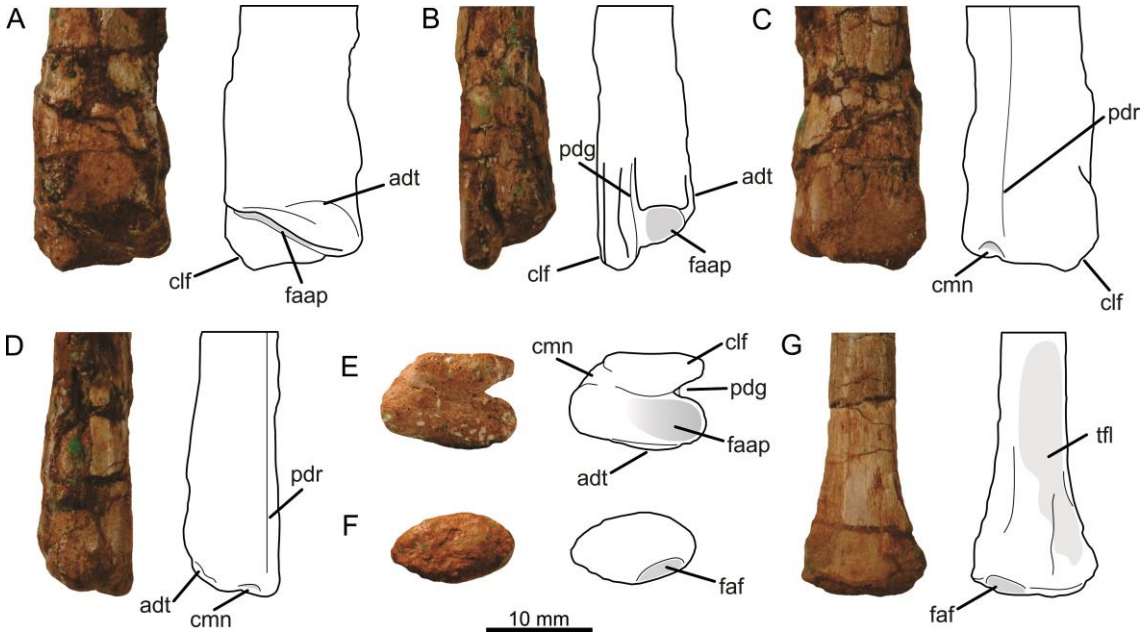

FIGURE 11. *Nhandumirim waldsangae* gen. et sp. nov. (LPRP/USP 0651). Distal end and outline drawings of right tibia (**A-E**) and fibula (**F** and **G**) in (**A**) cranial, (**B**) lateral, (**C**) caudal, (**D** and **G**) medial and (**E** and **F**) distal views. **Abbreviations**: **adt**, anterior diagonal tuberosity; **clf**, caudolateral flange; **cmn**, caudomedial notch; **faap**, articular facet for the ascending process of the astragalus; **faf**, articular facet in distal fibula; **pdg**, proximodistally oriented groove; **pdr**, proximodistally oriented ridge; **tfl**, insertion area for the tibiofibular ligament. [planned for page width]

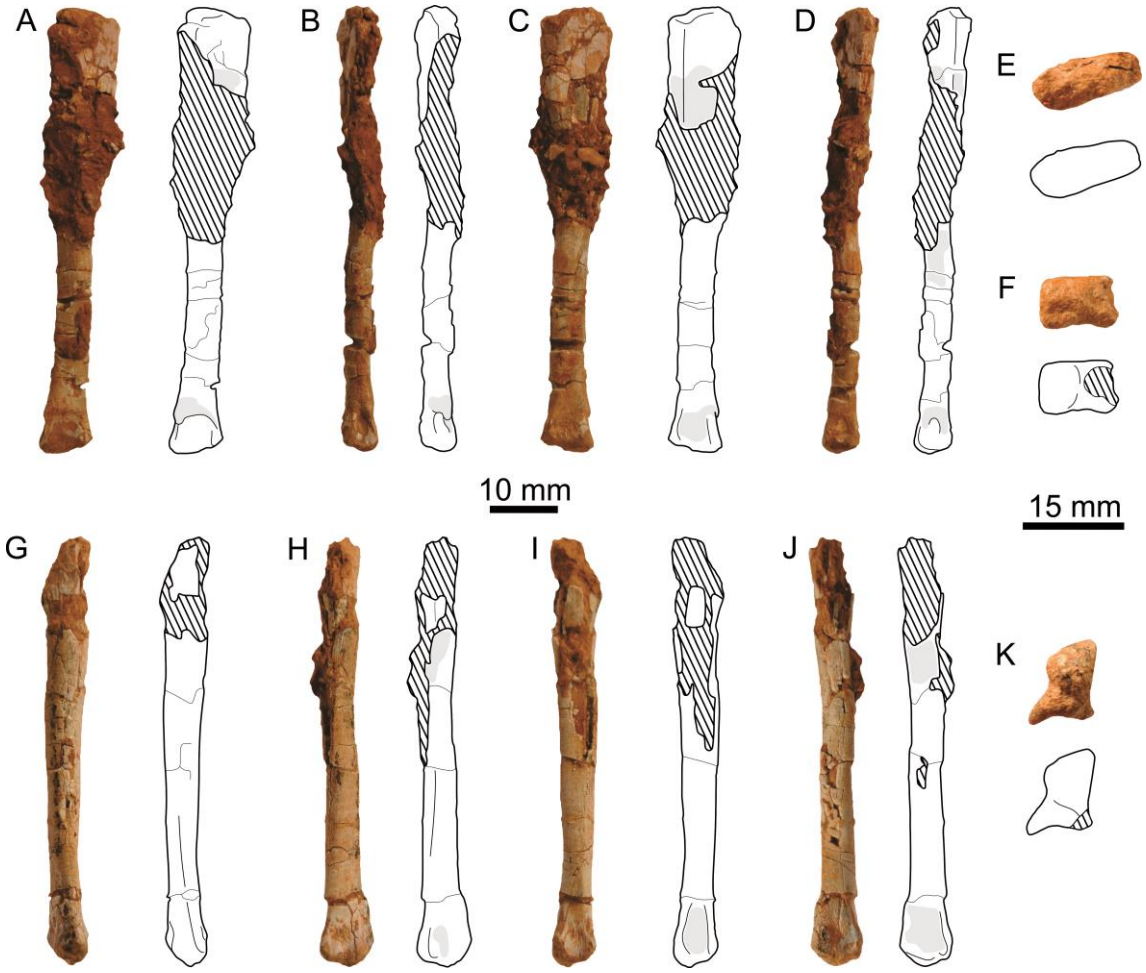

FIGURE 12. *Nhandumirim waldsangae* gen. et sp. nov. (LPRP/USP 0651). Right metatarsals II (**A**-**F**) and IV (**G**-**K**) in (**A** and **G**) cranial, (**B** and **H**) lateral, (**C** and **I**) caudal, (**D** and **J**) medial, (**E**) proximal and (**F** and **K**) distal views. Light grey indicates scarred areas, and cross-hatched areas represent broken portions. [planned for page width]

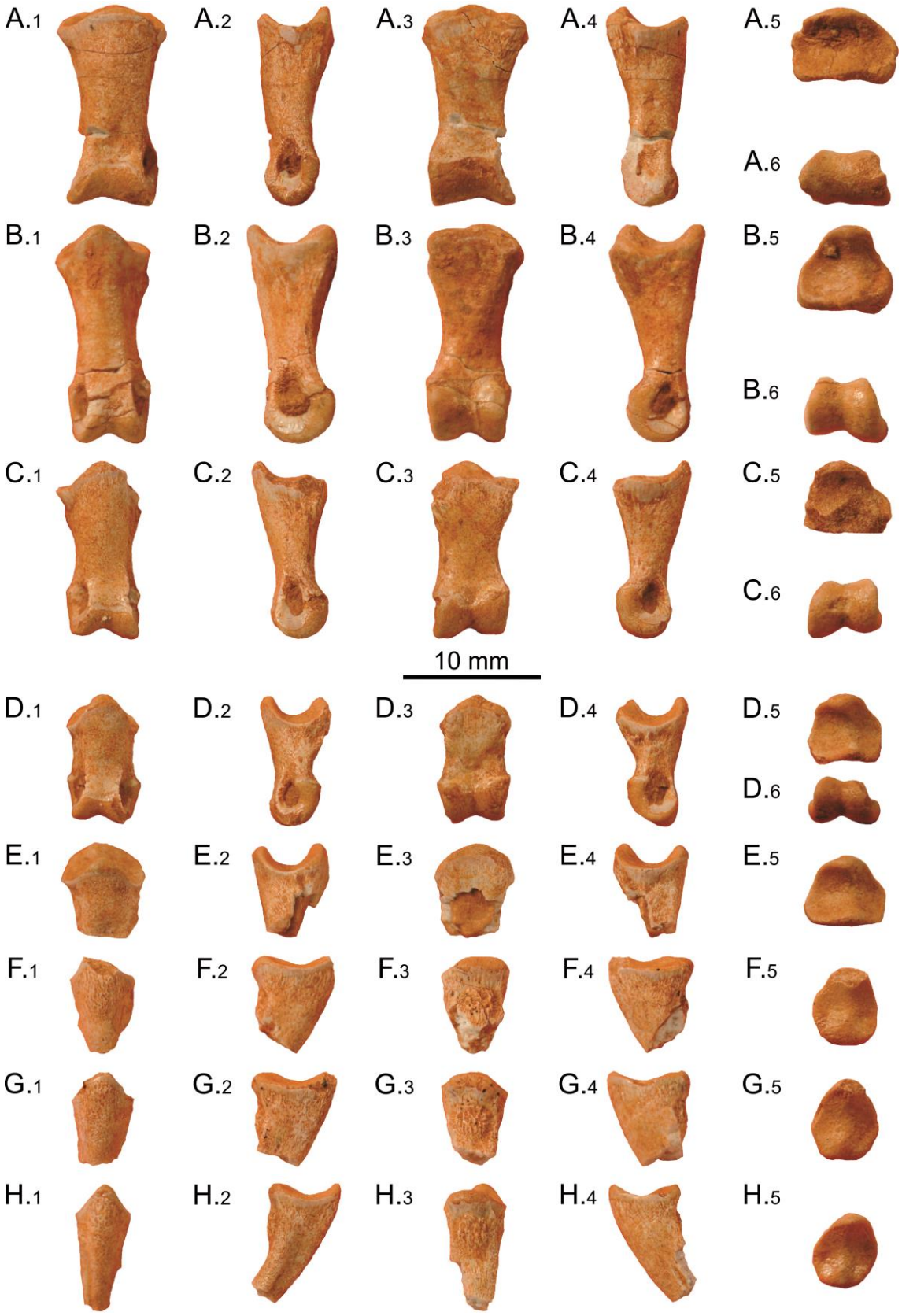

FIGURE 13. *Nhandumirim waldsangae* gen. et sp. nov. (LPRP/USP 0651). Right pedal phalanges in (**A_1-H_1**) dorsal, (**A_2-H_2**) lateral, (**A_3-H_3**) plantar, (**A_4-H_4**) medial, (**A_5-H_5**)

proximal and (**A6-D6**) distal views. Non-ungual phalanges 1-5 are respectively represented in **A-E**. **F-G** represent the unguals. [planned for page width]

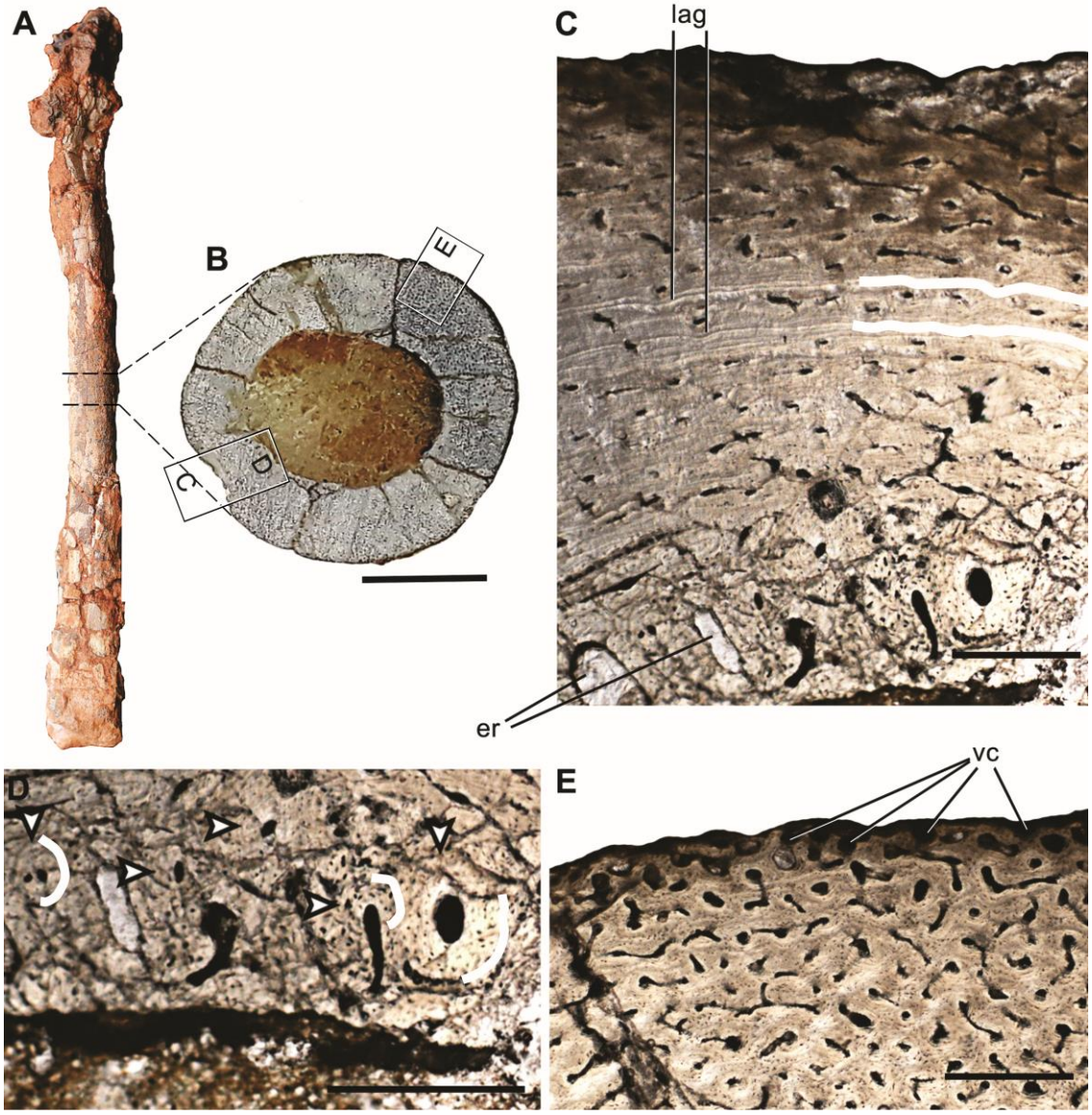

FIGURE 14: General microstructural anatomy of the tibia of *Nhandumirim waldsangae* gen. et sp. nov. (LPRP/USP 0651). **(A)** Right tibia indicating the sampled area of the bone. (**B**) Cross section of the tibia with the squared areas detailed in (**C-E**). (**C**) View of the complete transect showing the osteohistological pattern of the tibia, with two lines of arrested growth in the middle cortex marked by white lines, and erosion cavities indicating the beginning of remodelling process in the deep cortex. (**D**) Arrows point to

secondary osteons, also marked by white lines. (**E**) Detail of the vascular arrangement, highlighting the vascular canals reaching the periosteal surface. Scale bars: 100mm (**B**); 200µm (**C**, **E**); 250µm (**D**). **Abbreviations**: **er**, erosion cavities; **lag**, line of arrested growth; **vc**, vascular canals. [planned for page width]

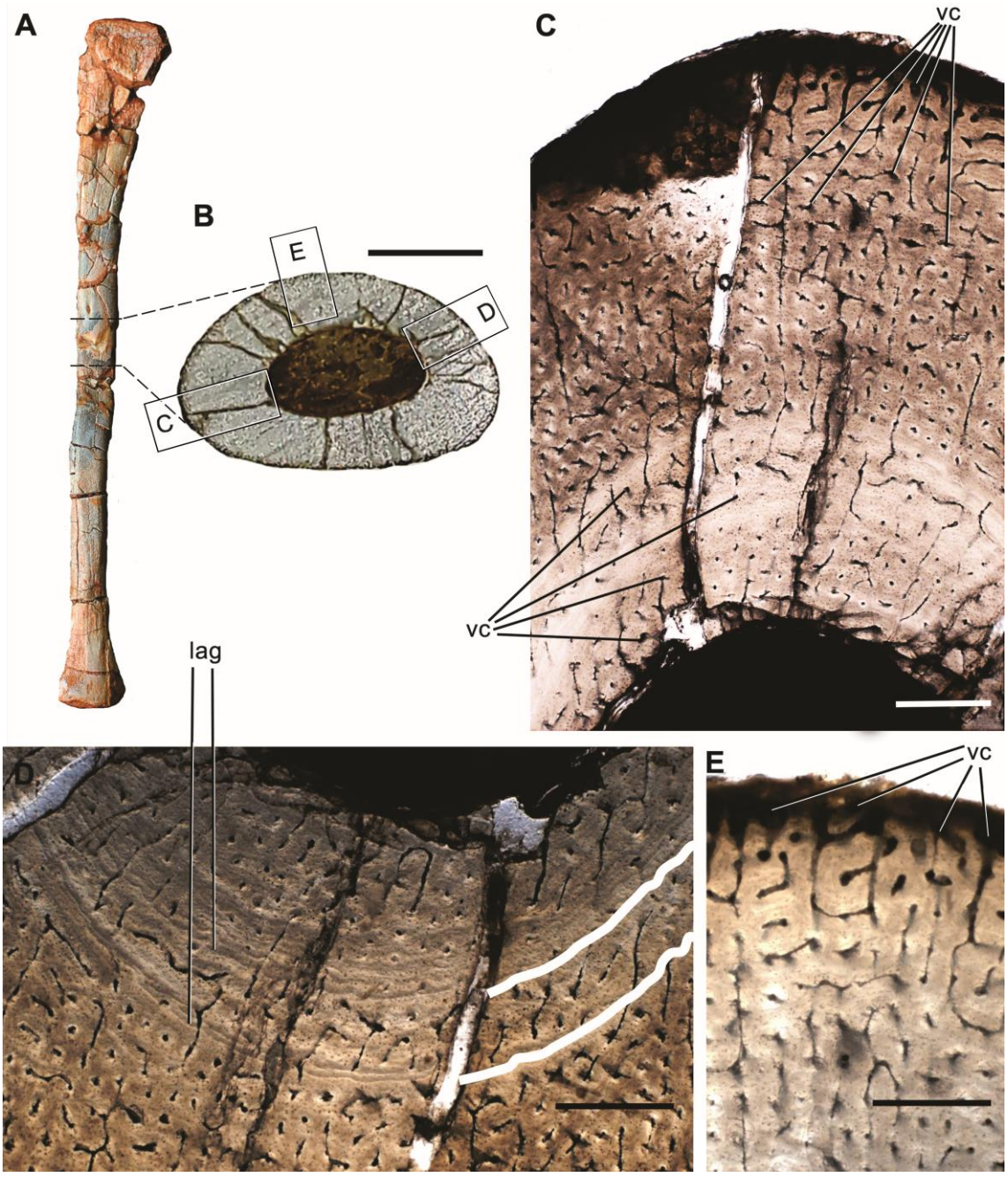

FIGURE 15. General microstructural anatomy of the fibula of *Nhandumirim waldsangae* gen. et sp. nov. (LPRP/USP 0651). **(A)** Right fibula indicating the sampled

area of the bone. (**B**) Cross section of the fibula with the square areas detailed in (**C**-**E**). (**C**) View of the complete transect showing the osteohistological pattern of the fibula, composed by plexiform arrange of the vascular network. (**D**) Lines of arrested growth in the middle cortex marked by white lines. (**E**) Detail of the vascular arrangement, highlighting the vascular canals reaching the periosteal surface. Scale bars: 150mm (**B**); 250µm (**C**); 300µm (**D**-**E**). **Abbreviations**: lag, line of arrested growth; **vc**, vascular canals. [planned for page width]

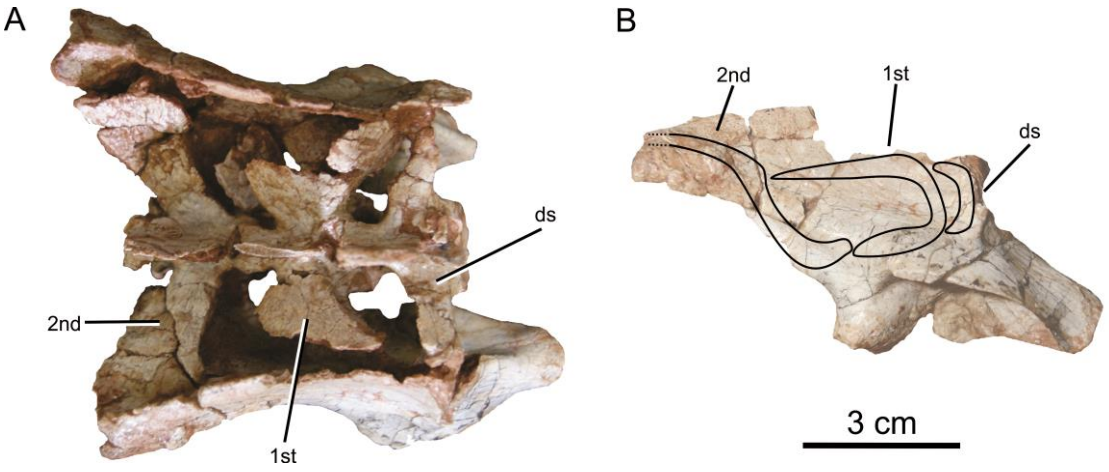

FIGURE 16. *Saturnalia tupiniquim* (MCP-3845 PV). Articulated sacrum and ilia in dorsal (**A**) view. **B.** Outline drawings represent the lateral aspect of the attachment scars of the sacral vertebra transverse processes and ribs in the right ilium. **Abbreviations**: **1st**, first primordial sacral vertebra; **2nd**, second primordial sacral vertebra; **ds**, dorsal vertebra incorporated to the sacrum. [planned for page width]

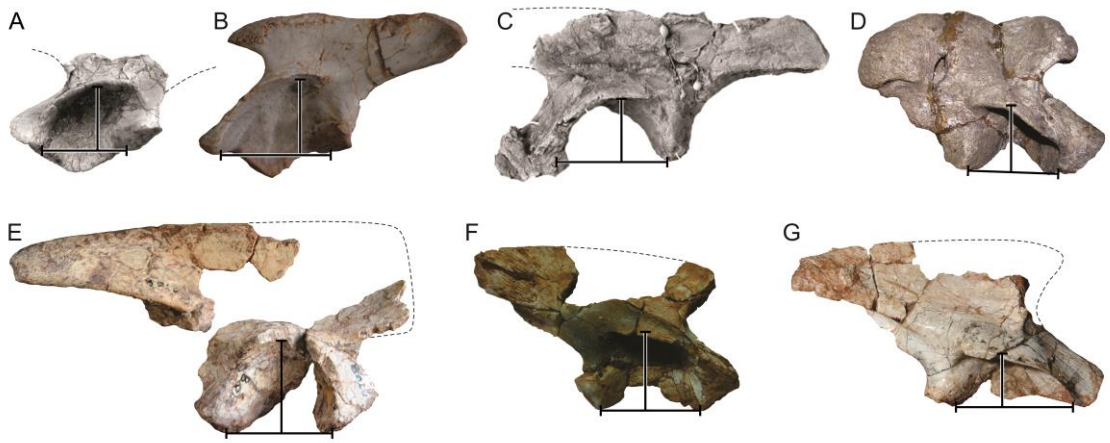

FIGURE 17. Lateral view of several early dinosauromorph ilia, showing the depth of the acetabulum. Dashed lines represent the possible limits of missing parts. **A**, *Asilisaurus kongwe* (NMT RB159, after Peecook et al., 2013); **B**, *Ixalerpeton polesinensis* (ULBRA-PVT059); **C**, *Eocursor parvus* (SAM-PK-K8025, after Butler, 2010); **D**, *Herrerasaurus ischigualastensis* (PVL 2566); **E**, *Coelophysis bauri* (AMNH FARB 2708); **F**, *Nhandumirim waldsangae* gen. et sp. nov. (LPRP/USP 0651); **G**, *Saturnalia tupiniquim* (MCP-3845 PV). Specimens scaled to the same acetabular length. [planned for page width]

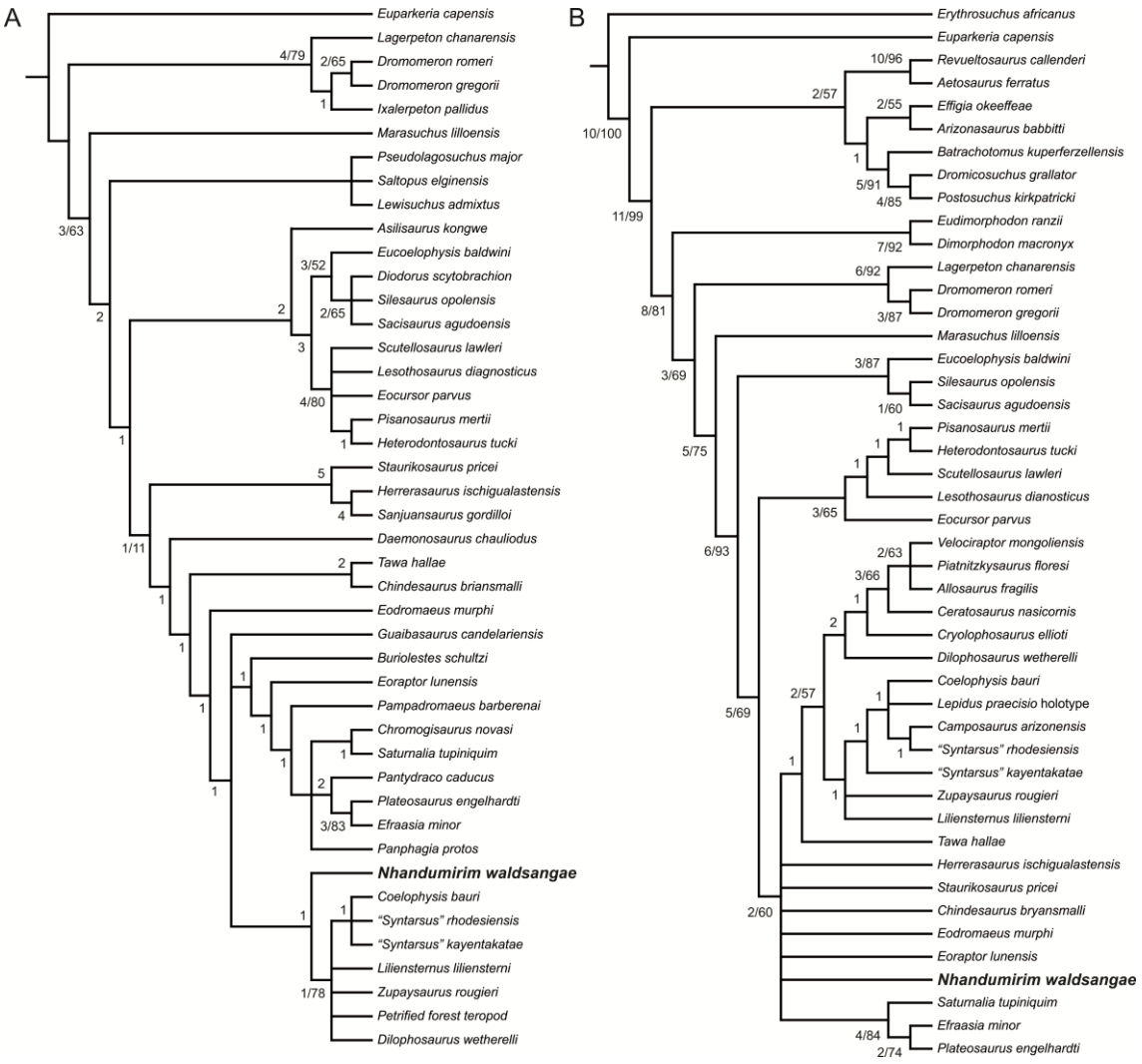

FIGURE 18. Phylogenetic relationships of *Nhandumirim waldsangae* gen. et sp. nov. (LPRP/USP 0651) among early dinosauromorphs. **A**, Strict consensus of 48 MPTs found in the analysis of the data matrix of Cabreira et al (2016); **B**, Strict consensus of 48 MPTs found in the analysis of the data matrix of Nesbitt and Ezcurra (2015). Values at nodes are Bremer support and bootstrap proportions (above 50%). [planned for page width]